Publications of the FTIA
32/2020

Finnish Transport Infrastructure Agency

FINITE ELEMENT MODELLING OF EARTH PRESSURE ON ABUTMENT PILES OF INTEGRAL BRIDGES

Finite element modelling of earth pressure on abutment piles of integral bridges

Publications of the FTIA 32/2020

Finnish Transport Infrastructure Agency

Helsinki 2020

Online publications pdf (www.vayla.fi)
ISSN 2490-0745
ISBN 978-952-317-785-7

Finnish Transport Infrastructure Agency
P.O.Box 33
FIN-00521 HELSINKI, Finland
Tel. +358 (0)295 34 3000

Foreword

This study was prepared by Ramboll Finland Ltd on behalf of Finnish Transport Infrastructure Agency (FTIA). The objective of the study was modelling the earth pressure on abutment piles of integral bridges with finite element analyses. The results were converted to a simplified analytical calculation model to be used in structural design of integral bridges.

The study was carried out by Marco D'Ignazio, PhD, Ville Lehtonen, PhD and Lauri P. Savolainen, MSc, from Ramboll Finland Ltd. The study was supervised by Veli-Matti Uotinen and Panu Tolla from FTIA.

Helsinki, December 2020

Finnish Transport Infrastructure Agency

Contents

1 Introduction

Väylävirasto (hereinafter referred to as Väylä or the Client) has asked Ramboll Finland Oy (Ramboll) to perform a study aiming to model the earth pressure on abutment piles of integral bridges. Bridge abutments are often founded on piles, especially in presence of difficult soil conditions.

Structural design of piles is strongly affected by the earth pressure acting along the piles during the construction of the road embankment and superstructure and under the action of traffic loads. The mobilized earth pressure is commonly determined analytically based on the simplified solution in Sillan geotekniset suunnitteluperusteet ("Geotechnical design criteria for bridges", Tiehallinto 2007). This solution accounts for the weight of the soil above the pile and the applied traffic load. The resulting earth pressure increment is calculated based on the earth pressure coefficient at rest (K_o) of the embankment/superstructure material and assuming a 2:1 stress distribution with depth.

Soil conditions and drainage during loading are expected to have an impact on the actual earth pressure. These aspects cannot be captured by the simplified analytical solution. Therefore, this study aims to compare the analytical approach to 3D Finite Element (FE) analyses carried out with the FE software PLAXIS 3D by Bentley.

Väylä provided Ramboll with the following inputs to be considered in the analyses:

Two bridge configurations:
- Integral bridge with cantilever span (hereinafter referred to as Cantilever or CA) and n.2 piles with diameter D=0,813m and 5m spacing
- Integral bridge without cantilever span (hereinafter referred to as Non-Cantilever or NCA) and n.2 piles with diameter D=0,813m and 5m spacing

A 5m-high embankment with additional 3m-high superstructure with 10m top width is considered. Two embankment configurations are modelled assuming:
- Crushed rock material with 1:1,5 slope
- Sand material with 1:2 slope

Two subsoil types are considered:
- Medium dense to dense sand with a friction angle $\varphi' = 36°$
- Clay with undrained shear strength $s_u = 40$ kPa

Surface loads as follows:
- Traffic loads: 9 kPa distributed, 9+31 (3x5m) kPa according to NCCI 7 (FTA Guidelines 13/2007)
- Train LM-71 max load: 52 (3x6,4m) kPa + 27 kPa (3m width); 52 (3x6,4m) load on bogies – repeated at 6,1m distance (RATO 3, FTA guidelines 13/2018)

All the necessary input parameters to the FE analyses are selected based on inputs from Väylä, available literature and Ramboll's experience. The proposed parameters are anticipated to represent best estimate properties. Therefore, the modelled earth pressure is also intended to represent a best estimate.

The analytical solution, the problem framework, the adopted geometries and assumptions, material models and parameters and FE results are presented and discussed in this report. Furthermore, a suggestion to improve the current analytical solution is briefly presented. Finally, the outcomes and limitations of this study are summarized, along with recommendations for future research work.

2 Analytical solution for earth pressure on abutment piles of integral bridges

Figure 2-1 shows the analytical solution for modelling earth pressure increments acting on bridge abutment piles contained in the "Geotechnical design criteria for bridges" guide that is used in Finland (Tiehallinto 2007).

The solution considers the unit weight (γ) and the earth pressure coefficient at rest (K_o) of the embankment/superstructure material located above the pile heads, over a height H. Further, it accounts for the effects of traffic loads (P).

As shown in Figure 2-1, being z the vertical coordinate, the earth pressure increments at z = H induced by the superstructure (P1) and the traffic load (P2) are calculated as follows:

$$P1 = \gamma \cdot H \cdot K_o \quad (1)$$

$$P1' = P1 \cdot B/(B+z) \quad (2)$$

$$P2 = P \cdot K_o \quad (3)$$

$$P2' = P2 \cdot B/(B+z) \quad (4)$$

The earth pressure distribution along the piles is calculated following a 2:1 load distribution with depth and according to the top width of the superstructure (B).

Further, the solution assumes that:

- The earth pressure is "gathered" from a 3-pile-diameter width, meaning that the analytical curves should be multiplied by a factor of three.
- The earth pressure increment is negligible below a depth of 1,2h from the top of the superstructure, where h is the thickness of the embankment + superstructure.

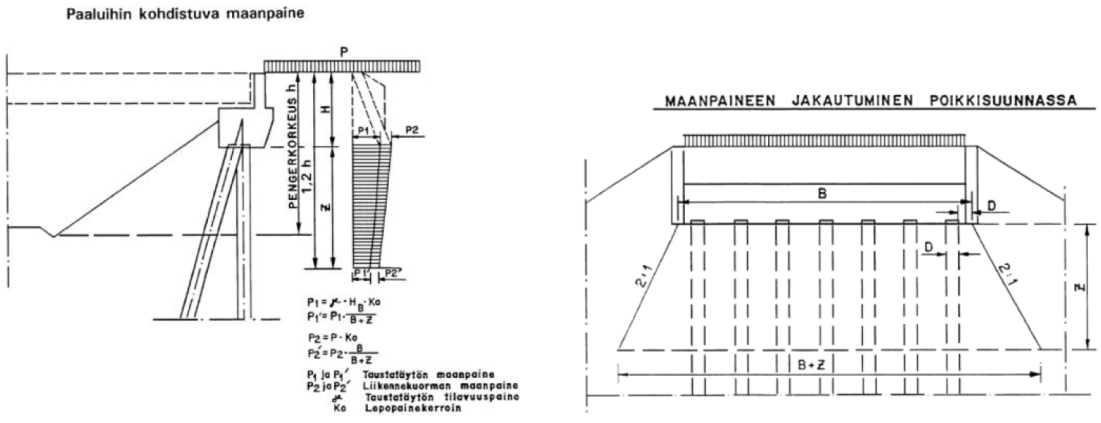

Figure 2-1 Analytical solution for earth pressure increments on abutment piles – Excerpt from the "Geotechnical design criteria for bridges" guide ("Sillan geotekniset suunnitteluperusteet", Tiehallinto 2007).

3 Definition of problem framework

3.1 Geometries

Figure 3-1 shows the reference geometries used in this study, based on the input from Väylä. A 5m-thick embankment with 3m-high superstructure is considered on top of an 8m-thick subsoil (sand or clay) resting over a 3m-thick moraine layer. The embankment slope is 1:1,5 for crushed rock and 1:2 for sand embankment. The groundwater table (GWT) is set 1,5 m below the subsoil surface. N.2 piles with D=0,813m are modelled with a 5m-spacing. The piles are 15m (NCA) and 17m (CA) long with 2m embedment in the deep moraine layer.

The pile head is modelled as fully fixed in the NCA case. Fully fixed and fully free pile head conditions are analysed for the CA case. The reason is that these would describe different scenarios of bearing on top of the pile. As communicated by Anssi Laaksonen (2020, personal communication to Ramboll and Väylä), the bearing on top of the pile should not be modelled as a spring, but rather assuming a constant friction. In any case, the friction is relatively low already in the case of a new bearing (friction coefficient ≈0,06), and it reduces to almost zero for an old bearing (≈0,002). Given that friction forces are negligible compared to the expected earth pressures, the pile head is modelled as both fully free and fully fixed to evaluate the effect of pile head fixity on the behaviour.

The loads are applied 2m from the abutment wall (as way of simplifying the effect of the transition slab). The distance between the pile centreline and the abutment wall is 0,6m and 2m for the NCA and CA layouts, respectively.

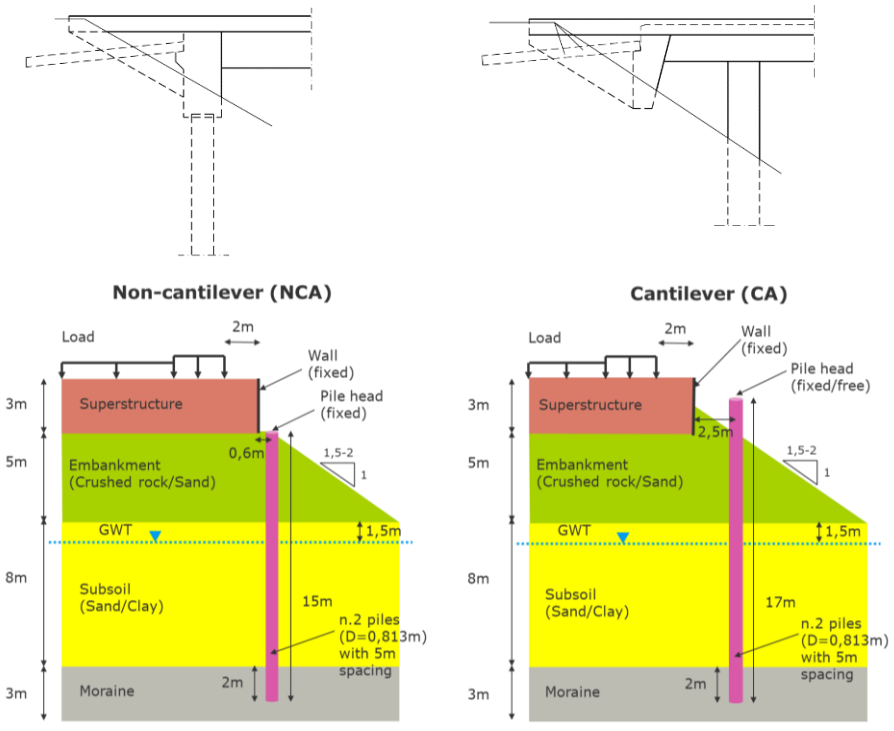

Figure 3-1 Schematization of NCA and CA bridge abutments with piles used in this study (not in scale). Line schematics from Väylä (2020).

3.2 Loads

The loads considered in this study are:
- Traffic loads: 9 kPa distributed, 9+31 (3x5m) kPa - NCCI 7 (FTA guidelines 13/2007)
- Train LM-71 max load: 52 (3x6,4m) kPa + 27 kPa (3m width); 52 (3x6,4m) load on bogies – repeated at 6,1m distance (RATO 3, FTA guidelines 13/2018)

3.3 Calculation matrix

The calculation matrix presented in Table 3-1 summarizes all the different calculations that are carried out. A progressive number and an ID are assigned to each calculation, according to the following nomenclature:

Bridge type - Embankment material - Subsoil & Pile-head fixity - Load type

Legend:
Bridge type: **CA** for cantilever; **NCA** for non-cantilever
Embankment material: **01** for crushed rock with 1:1,5 slope; **02** for sand with 1:2 slope
Subsoil: **S** for sand; **C** for clay
Pile-head fixity: **1** for fully fixed; **2** for fully-free
Load type: **T** for traffic load (9 + 31 kPa); **R1** for distributed 52 kPa+27 kPa LM-71 load; **R2** for 52 kPa LM-71 load on bogies

For instance, a cantilever bridge with a crushed rock embankment, clay subsoil, free pile head and traffic load reads as CA-01-C2-T; whereas a non-cantilever bridge with a sand embankment, sand subsoil, fixed pile head and distributed LM-71 load reads as NCA-02-S1-R1.

Table 3-1 Calculation matrix.

Bridge type	Embankment	Subsoil	Pile-head fixity	Load	ID	N.
Cantilever	Crushed rock	Sand	Fixed	9+31 kPa	CA-01-S1-T	1
				LM-71 v1	CA-01-S1-R1	2
				LM-71 v2	CA-01-S1-R2	3
			Free	9+31 kPa	CA-01-S2-T	4
				LM-71 v1	CA-01-S2-R1	5
				LM-71 v2	CA-01-S2-R2	6
		Clay	Fixed	9+31 kPa	CA-01-C1-T	7
				LM-71 v1	CA-01-C1-R1	8
				LM-71 v2	CA-01-C1-R2	9
			Free	9+31 kPa	CA-01-C2-T	10
				LM-71 v1	CA-01-C2-R1	11
				LM-71 v2	CA-01-C2-R2	12
	Sand	Sand	Fixed	9+31 kPa	CA-02-S1-T	13
				LM-71 v1	CA-02-S1-R1	14
				LM-71 v2	CA-02-S1-R2	15
			Free	9+31 kPa	CA-02-S2-T	16
				LM-71 v1	CA-02-S2-R1	17
				LM-71 v2	CA-02-S2-R2	18
		Clay	Fixed	9+31 kPa	CA-02-C1-T	19
				LM-71 v1	CA-02-C1-R1	20
				LM-71 v2	CA-02-C1-R2	21
			Free	9+31 kPa	CA-02-C2-T	22
				LM-71 v1	CA-02-C2-R1	23
				LM-71 v2	CA-02-C2-R2	24
Non-Cantilever	Crushed rock	Sand	Fixed	9+31 kPa	NCA-01-S1-T	25
				LM-71 v1	NCA-01-S1-R1	26
				LM-71 v2	NCA-01-S1-R2	27
		Clay	Fixed	9+31 kPa	NCA-01-C1-T	28
				LM-71 v1	NCA-01-C1-R1	29
				LM-71 v2	NCA-01-C1-R2	30
	Sand	Sand	Fixed	9+31 kPa	NCA-02-S1-T	31
				LM-71 v1	NCA-02-S1-R1	32
				LM-71 v2	NCA-02-S1-R2	33
		Clay	Fixed	9+31 kPa	NCA-02-C1-T	34
				LM-71 v1	NCA-02-C1-R1	35
				LM-71 v2	NCA-02-C1-R1	36

Legend		
Crushed rock	01	1:1,5 slope
Sand	02	1:2 slope
Sand	S	
Clay	C	
Fixed	1	
Free	2	
Traffic	T	
Railway	**R**	
Distributed	1	
Bogies	2	

4 Finite element model

4.1 Geometry and mesh

Figure 4-1 and Figure 4-2 show the 3D Plaxis models for CA and NCA bridge abutments, respectively, including soil layering and all the elements, model dimensions and FE mesh. The soil volumes are modelled with 10-noded elements and the mesh consist of around 35 000 elements. Despite the model's symmetry along the y-axis, the full model was required for the analyses because of the non-symmetric traffic load applied.

Standard deformation boundary conditions are applied to the 3D model, meaning that the model base is set as fully fixed and the top surface is free to move, while the lateral boundaries are normally fixed against horizontal displacements (roller conditions).

The piles (D=0,813m) are modelled as linear elastic solid elements. Their top connection to the bridge is modelled by means of surface displacements set to simulate top fixities (fully fixed or fully free head). The top of the pile is set at z=-1m for CA and z=-3m for NCA. The piles are embedded 2m into a 3m-thick moraine layer. This is to ensure that the bottom fixity of the pile is modelled in a realistic way, compared to e.g. fully fixed connection. Further, interface elements are modelled between the piles and the surrounding soil to ensure that the strength at the interface is reduced compared to the intact adjacent soil.

The embankment with superstructure is modelled up to a height of 8 m above the subsoil, between z=0m and z=-8m. The 8m-thick subsoil goes from z=-8m and z=-16m. A 3m-thick moraine layer is modelled between z=-16m and z=-19m.

The abutment walls are modelled by means of rigid surfaces that prevent movements in all direction. Friction between walls and the surrounding soil is modelled by means of interface elements. The distance between the piles centreline and the front wall is 0,6m for NCA and 2,5m for CA.

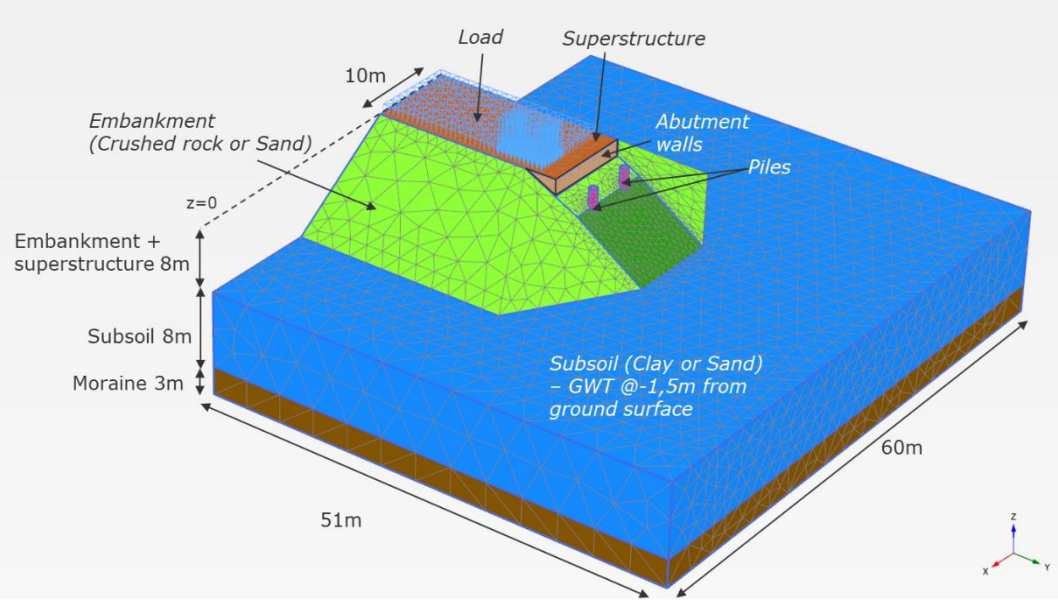

Figure 4-1 FE geometry and mesh – Cantilever (CA) model.

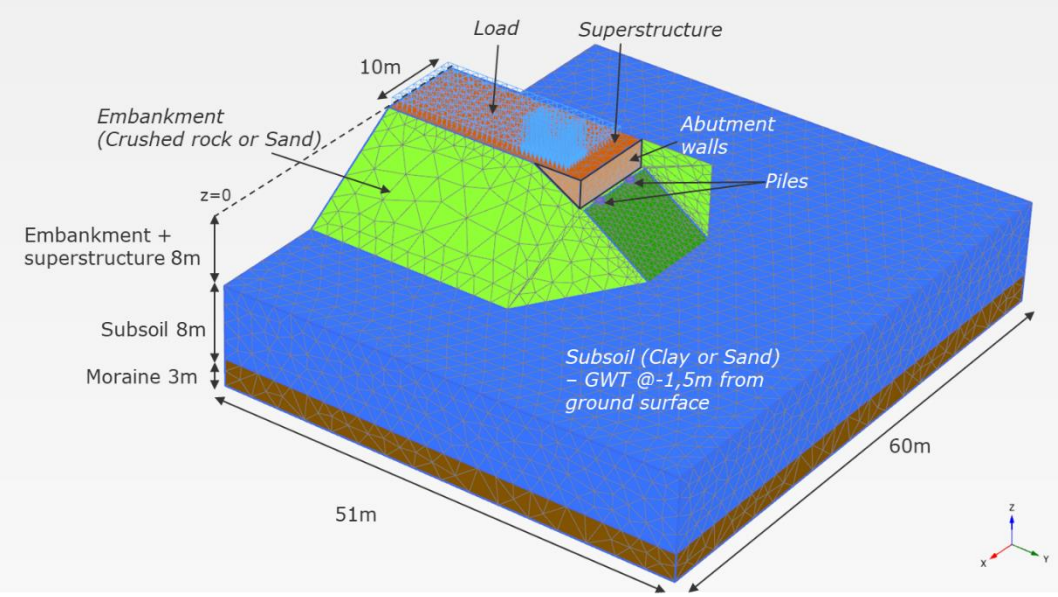

Figure 4-2 FE geometry and mesh – Non-Cantilever (NCA) model.

4.2 Load configurations

Loads are applied as distributed surface loads. The traffic load is applied at z=0m (surface) and at 2m distance from the front abutment wall, both for CA and NCA layouts. The load is non-symmetric and is applied as shown in Figure 4-3. The maximum vertical load of 40 kPa is applied over an area of 3m x 5m (x_{min} = 1,5m; x_{max}=4,5m) at 2m distance from the abutment wall. A distributed load of 9 kPa is applied everywhere else. This configuration is referred to as "base case". Further, the 40 kPa load is applied at (x_{min} = -1,5m; x_{max}=1,5m) and (x_{min} = -4,5m; x_{max}=-1,5m). The effect of the maximum load location on the pile behaviour is discussed later in section 0

The train LM-71 loads are applied at z=-0,5m and at 2m distance from the front wall for both NCA and CA. The loads are symmetric and is applied as shown in Figure 4-4. The maximum load of 52 kPa is applied over 3m x 6,4m (x_{min} = 0,75; x_{max}=3,75m and x_{min} = -3,75; x_{max}=-0,75m). A load of 27 kPa is applied over the same width and for the whole extent of the superstructure.

The 52 kPa bogies load is applied over 3m x 6,4m (x_{min} = 0,75; x_{max}=3,75m and x_{min} = -3,75; x_{max}=-0,75m). The load is repeated at a 6,1m distancing in y-direction, as shown in Figure 4-4.

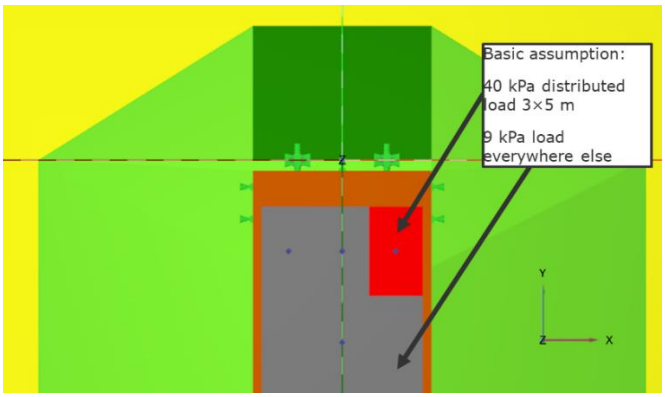

Figure 4-3 Configuration of traffic load - NCA.

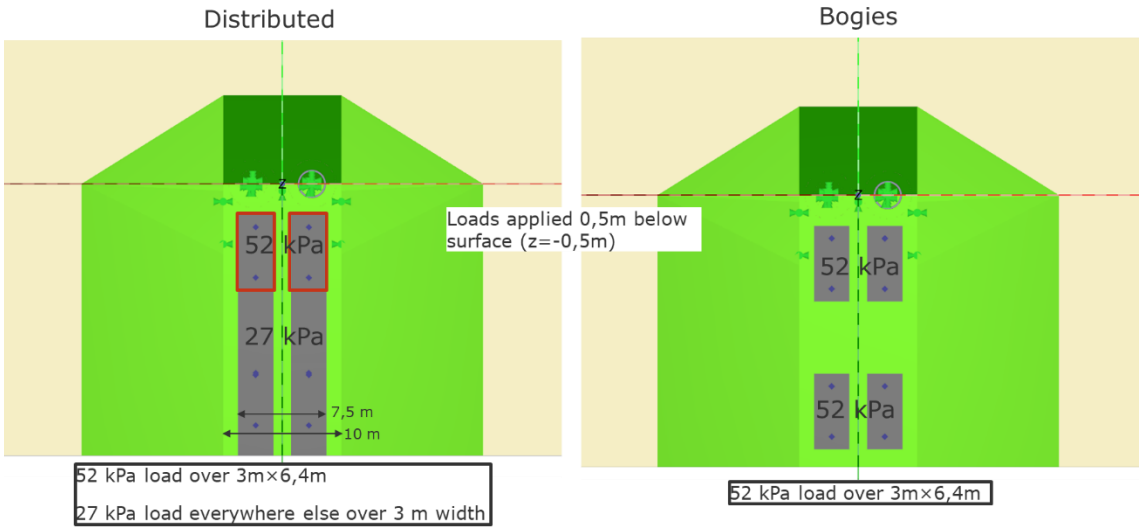

Figure 4-4 Configuration of LM-71 load - NCA.

4.3 Construction phases and calculation steps

Figure 4-5 shows the construction phases of the embankment, piles and superstructure and the calculation steps to model earth pressure on piles under the different loads for the situation where the subsoil is sand. The initial stresses in the subsoil are generated through a "K_o phase", where the soil weight is applied, and stresses are defined according to K_o.

The 5m embankment is modelled as a drained material and applied by gravity in a plastic calculation phase (1a). This will result in mobilized shear stress in the embankment and stress change in the drained subsoil. The mobilized shear in the embankment is affected by the deformations in the subsoil. In a subsequent phase (1b), piles are activated. This represents a phase where no mobilization of earth pressure is generated along the piles, since those are activated (in reality, installed) only after the embankment construction.

In phase 2, the 3m superstructure and loads are applied. Firstly, the 3m superstructure, modelled as drained, is applied and the earth pressure mobilized (2a). Secondly, additional earth pressure mobilization occurs under the applied load (2b).

Figure 4-6 shows the construction phases of the embankment, piles and superstructure and the calculation steps to model earth pressure on piles under the different loads for the situation where the subsoil is clay. The initial stresses in the subsoil are generated through a "K_o phase", where the soil weight is applied, and stresses are defined according to K_{ONC} and a POP. The clay is modelled as Drained.

The 5m embankment is modelled as a drained material and applied by gravity in a plastic calculation phase (1a). This will result in mobilized shear stress in the embankment and stress change in the drained subsoil. The mobilized shear in the embankment is affected by the deformations in the subsoil. Compared to the sand case, the embankment deformations are anticipated to be significantly larger (≈2 orders or magnitude). In a subsequent phase (1b), piles are activated. This represents a phase where no mobilization of earth pressure is generated along the piles, since those are activated (in reality, installed) only after the embankment construction.

In phase 2, the clay behaviour is switched to undrained and 3m superstructure and loads are applied. Firstly, the 3m superstructure, modelled as drained, is applied and the earth pressure mobilized both from the embankment and the undrained clay (2a). Secondly, additional earth pressure mobilization occurs under the applied load (2b).

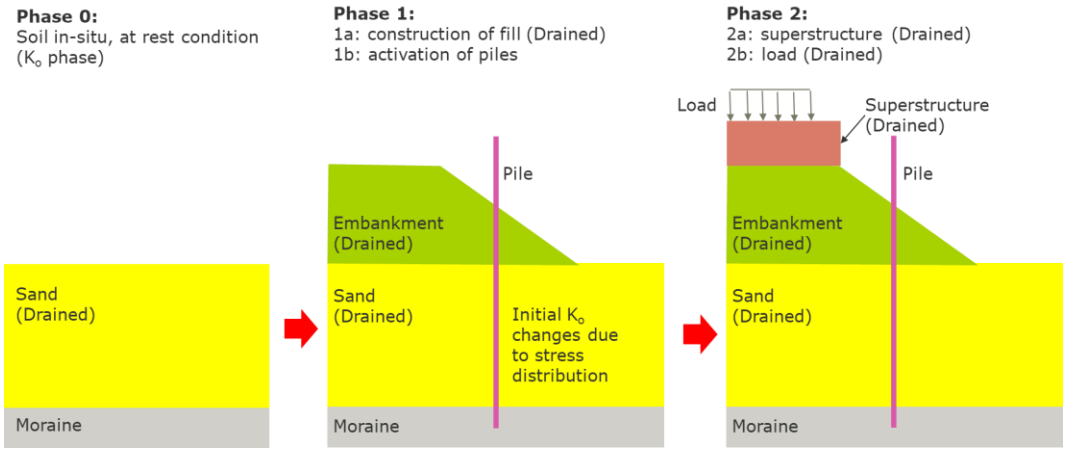

Figure 4-5 Calculation steps – Sand subsoil (not in scale).

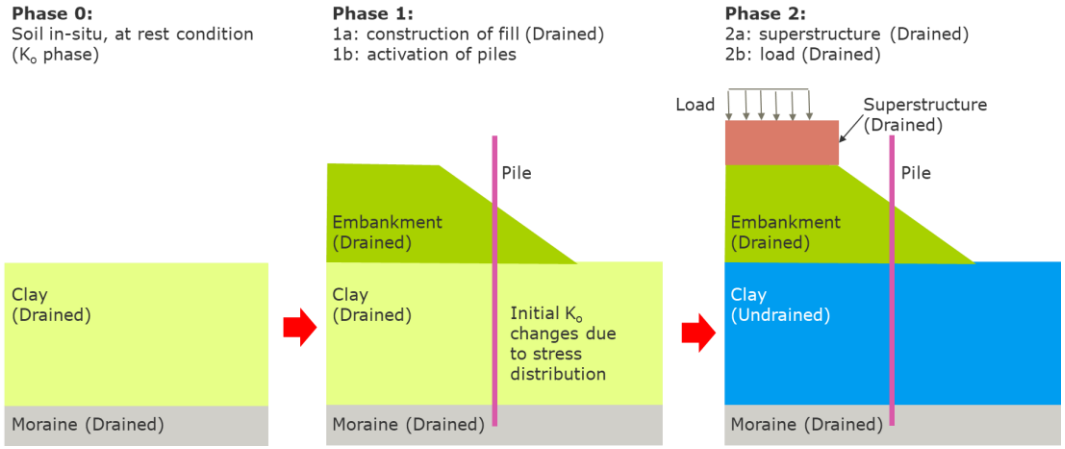

Figure 4-6 Calculation steps – Clay subsoil (not in scale).

4.4 Earth pressure modelling

The earth pressure along the piles is modelled as the average stress acting on a surface right behind the pile. The surface width is taken equal to the pile diameter D = 0,813 m. The reference surface is normal to the maximum displacement direction, which is inclined by an angle α from the x-direction. The concept is illustrated in Figure 4-7:

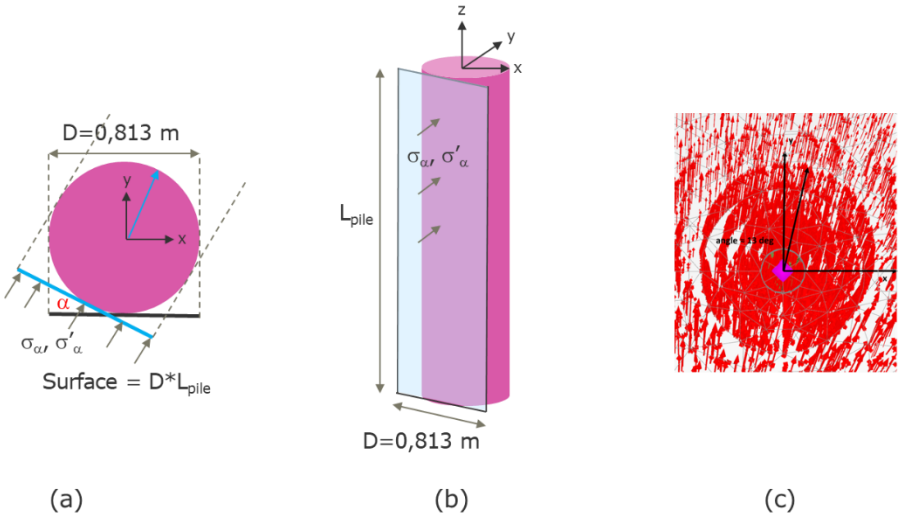

Figure 4-7 Selection of reference surface for modelling earth pressure acting along piles (a) top view and (b) 3D view. (c) Displacement vector under traffic load (CA-01-S1-T).

In general, α ranges between 10 and 15° for all the calculations. An example is given in Figure 4-7c. For α = 10-15°, $\sigma_{max,a} = \sigma_{normal}/\cos\alpha = \sigma_{yy}/\cos\alpha \approx \sigma_{yy}$. Therefore, for simplicity, the stresses acting in the y-direction are taken to model earth pressure. For drained and undrained layers, σ'_{yy} (effective) and σ_{yy} (total) are used, respectively.

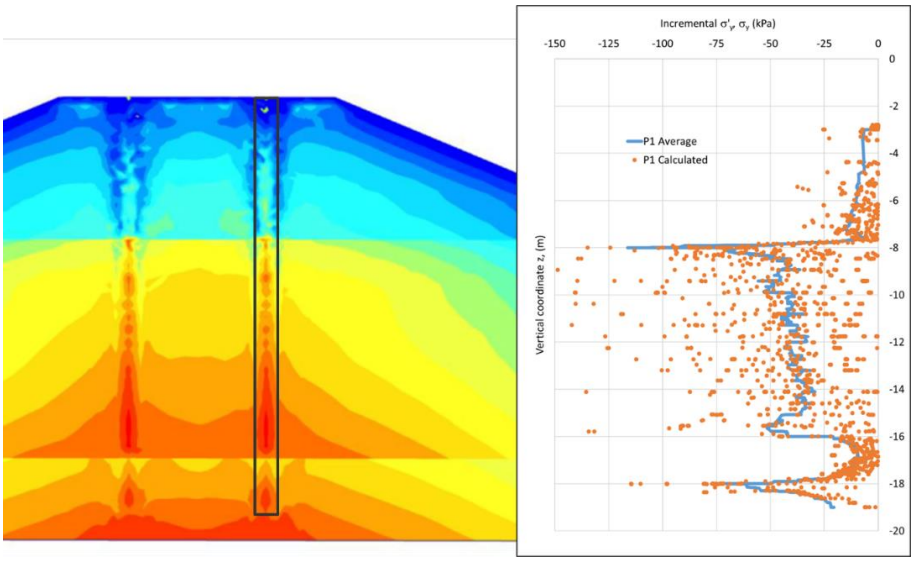

Figure 4-8 Illustration of cross-section used to model earth pressure and example of average earth pressure obtained for a point distribution across a surface with width equal to the pile diameter.

As shown in Figure 4-8, a large scatter characterizes the stress distribution across the surface. The scatter does not reduce significantly by improving the FE mesh around the pile. Hence, a moving average along the pile axis (z-axis) is calculated to define the average earth pressure acting along the pile.

5 Material models and parameters

Coarse materials that are expected to exhibit drained behaviour are modelled by the Hardening Soil model. These include the embankment, superstructure, sand subsoil and moraine. The Hardening Soil model is further used to simulate the long-term drained behaviour of the clay subsoil beneath the 5m embankment, prior to construction of the superstructure and application of the loads. The undrained behaviour of the clay subsoil is otherwise modelled by the Mohr-Coulomb model where the stiffness is selected so that it corresponds to fairy small strain levels. Piles are modelled as linear elastic volume elements. The following sections describe the basics of the material models used and the selection of model parameters.

Input parameters to the FE analyses are selected based on inputs from the Client, available literature and Ramboll's experience. The proposed parameters are anticipated to represent best estimate properties.

5.1.1 Hardening Soil model

The Hardening Soil (HS) model is an advanced model for simulating the behaviour of both soft soils and stiff soils (Plaxis, 2020). When subjected to primary deviatoric loading, soil shows a decreasing stiffness and simultaneously irreversible plastic strains develop. In the special case of a drained triaxial test, the observed relationship between the axial strain and the deviatoric stress can be well approximated by a hyperbola. The hyperbola tends asymptotically to the upper limiting deviator stress at failure q_a (Figure 5-1). Hence, the failure criterion should be defined so that the maximum deviator stress is lower than q_a to obtain reasonable strain level at failure. In the model formulation, q_f is limited by the Mohr-Coulomb failure criterion and it is by default assumed equal to $0.90q_a$.

The ultimate deviatoric stress, q_f, and q_a are defined as shown by equation (5) as:

$$q_f = (c' \cot\varphi' - \sigma'_3)\frac{2\sin\varphi'}{1-\sin\varphi'} \quad \text{and} \quad q_a = \frac{q_f}{R_f} \qquad (5)$$

where c' is the effective cohesion, φ' is the effective angle of internal friction and $\sigma'_3 = \sigma_3$-u is the minor principal stress, which represents the confining pressure in a triaxial test. The R_f default value is 0.90.

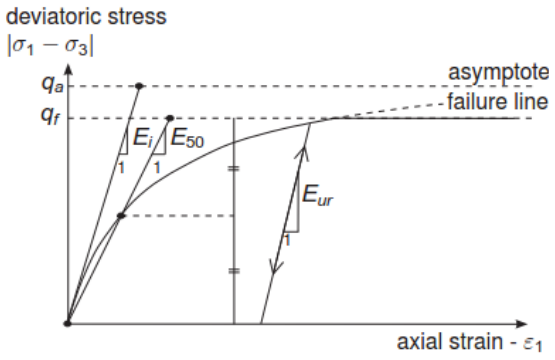

Figure 5-1 Hyperbolic stress-strain relation in primary loading for a standard drained triaxial test (Plaxis, 2020).

Some basic characteristics of the model are:

- Stress dependent stiffness according to a power law
  Input parameter m
- Plastic straining due to primary deviatoric loading
  Input parameter E_{50}^{ref}
- Plastic straining due to primary compression
  Input parameter E_{oed}^{ref}
- Elastic unloading / reloading
  Input parameters E_{ur}^{ref}, ν_{ur}
- Failure according to the Mohr-Coulomb failure criterion
  Parameters c', φ' and ψ

A basic feature of the HS model is the stress dependency of soil stiffness. For oedometer conditions of stress and strain, the model implies for example the relationship:

$$E_{oed} = E_{oed}^{ref} (\sigma' / p^{ref})^m \quad (6)$$

where E_{oed} is the oedometer modulus at a given stress level σ', E_{oed} is the oedometer modulus at a reference stress p^{ref} (a default p_{ref} = 100 kPa is used by Plaxis), *m* is the stress exponent defined as 1 – β (being β the Ohde-Janbu's stress exponent). The stiffness in primary drained triaxial loading E_{50} and the unloading/reloading stiffness E_{ur} are defined in a similar way as E_{oed}. More details can be found in the Plaxis' user's manual (Plaxis, 2020).

Typically, *m* ≈ 0,5 for coarse soils, while *m* ≈ 0,7 for silty soils. In the special case of soft soils, it is realistic to use *m* = 1.

A description of the Hardening Soil model parameters can be found in Table 5-1.

Table 5-1 Hardening Soil model parameters.

Parameter	Unit	Description
γ_{sat}	kN/m^3	Saturated unit weight
γ_{unsat}	kN/m^3	Unsaturated unit weight
E_{50}^{ref}	kPa	Secant stiffness in standard drained triaxial test at p^{ref}
E_{oed}^{ref}	kPa	Tangent oedometer stiffness at p^{ref}
E_{ur}^{ref}	kPa	Unloading/Reloading stiffness at p^{ref}
m	-	Power for stress-level dependency of stiffness
c′	kPa	Effective cohesion
ϕ'	o	Friction angle
ψ	o	Dilatancy angle
ν_{ur}	-	Poisson's ratio for unloading/reloading
p^{ref}	kPa	Reference stress for stiffness
K_o^{nc}	-	Normally consolidated K_o value
R_f	-	Failure ratio q_f / q_a
$\sigma_{tension}$	kPa	Tension cut-off and tensile strength
k_x, k_y, k_z	m/d	Hydraulic conductivity (or permeability) in x, y and z directions

Parameter	Unit	Description
e_0	-	Initial void ratio
c_k	-	Change of permeability coefficient
POP	kPa	Pre-overburden pressure
R_{inter}	-	Interface strength reduction coefficient

Generally, the symbol *m* is used to indicate the Ohde-Jabu's modulus number; while in the HS model, *m* represents the stress-exponent (= 1 – β). To avoid confusion, the modulus number is hereinafter indicated using the symbol *m**, while *m* is kept for the stress exponent. Hence, the stress-dependent moduli can be determined as shown in equations (7), (8) and (9) as:

$$E_{oed}^{ref} = m^* \cdot p^{ref} \quad (7)$$

$$E_{50}^{ref} \approx E_{oed}^{ref} \quad (8)$$

$$E_{ur}^{ref} = n \cdot E_{50}^{ref} \quad (9)$$

As described in the PLAXIS' manual, in many practical cases it is appropriate to set E_{ur}^{ref} equal to $3E_{50}^{ref}$; this is the default setting used in PLAXIS. Further, it is generally assumed that $E_{50}^{ref} \approx E_{oed}^{ref}$. However, the ratio between moduli should be defined based on laboratory test results, whenever possible. For the superstructure, $E_{ur}^{ref} = 2E_{50}^{ref}$ is assumed. For clay, $E_{ur}^{ref} > 10E_{50}^{ref}$.

Based on the Annex 6 in NCCI 7 (Liikennevirasto 2017), the modulus number m* is taken equal to 1100 for crushed rock and moraine, m*=500 as representative of a medium dense to dense sand. For the superstructure, m*=1350 was assumed based on Ramboll's experience. Other stiffness and strength parameters and soil weight are further assumed based on Ramboll's experience. For the clay, m*=9 is chosen according to Janbu (1998) for a water content of 75%. Stress exponents of 0,5 and 1 are assumed for coarse layers and clay, respectively.

Input parameters for the different soil units are summarized in Table 5-2.

Table 5-2 Input parameters for Hardening Soil model.

Parameter	Unit	Superstructure	Crushed rock	Sand	Moraine	Clay
γ_{unsat}	kN/m³	20	20	18	21	15,2
γ_{sat}	kN/m³	20	20	18	21	15,2
E_{50}^{ref}	MPa	160	120	50	120	0,9
E_{oed}^{ref}	MPa	135	110	55	110	0,9
E_{ur}^{ref}	MPa	320	360	150	360	18
c'	kPa	5	0,1	0,1	0,1	0,1
φ'	°	45	45	36*	40	25
ψ	°	5	5	6	10	0
ν_{ur}	-	0,2	0,2	0,2	0,2	0,2
m	-	0,5	0,5	0,5	0,5	1
p^{ref}	kPa	100	100	100	100	100

Parameter	Unit	Superstructure	Crushed rock	Sand	Moraine	Clay
K_0^{nc}	-	0,29	0,33	0,41	0,36	0,58
R_f	-	0,9	0,9	0,9	0,9	0,9
e	-	0,5	0,5	0,5	0,5	2
POP	kPa	0	0	0	0	20
R_{inter}	-	0,5	0,5	0,5	0,5	0,7
Drainage type	-	Drained	Drained	Drained	Drained	Drained

*Input from the Client

5.1.2 Mohr-Coulomb model

The Mohr-Coulomb (MC) model is an elastoplastic model for simulating both drained and undrained soil behaviour. The model assumes a constant stiffness and a linear-stress-strain behaviour before reaching the failure state. In this way, the stiffness is independent of both stress level and shear mobilization. The MC model is used to model the undrained response of the clay subsoil. As suggested by the Client, the 8m-thick clay unit is characterized by a constant undrained shear strength s_u = 40 kPa. The soil stiffness is then selected according to literature as a function of s_u and assuming a plasticity index (PI) of 30%.

According to Termaat et al. (1985), the shear modulus at 50% of the shear strength (G_{50}) can be defined as:

$$G_{50}/s_u = 5000/PI(\%) = 5000/30 \approx 167 \quad (10)$$

Further, a common formula to estimate the undrained elastic modulus E_u is:

$$E_u/s_u = 15000/PI(\%) = 15000/30 = 500 \quad (11)$$

Equations (10) and (11) give G = 6680 kPa and E_u = 20 000 kPa. The elasticity theory suggests that for E_u = 20 000 kPa and ν=0,495 (undrained), G = 6689 kPa. This is in line with equation (10).

Table 5-3 summarizes the input parameters for the Mohr-Coulomb model.

Table 5-3 Input parameters for Mohr-Coulomb model.

Parameter	γ_{unsat}	γ_{sat}	s_u	G/s_u	E_u/s_u	G	E_u	ν	R_{inter}	Drainage type
Unit	kN/m³	kN/m³	kPa	-	-	MPa	MPa	-	-	-
Clay	15,2	15,2	40*	167	500	6,7	20	0,495	0,7	Undrained (C)

*Input from the Client

5.1.3 Linear Elastic parameters for piles

The piles are modelled as circular linear elastic volume elements with an elastic modulus E = 42 GPa, Poisson's ratio ν = 0,3, unit weight γ = 28 kN/m^3 and diameter D = 0,813 m.

The input parameters are calculated for composite reinforced concrete RR800/12.5 piles with steel grade S440J2H. The pile is characterized by a steel

bundling frame A500HW, C35/45 concrete and n.18 Ø32 steel reinforcement bars, corresponding to a ≈3% reinforcement. This configuration, which is shown in Figure 5-2, gives a bending stiffness EI ≈ 900 MNm^2. For D = 0,813m, E ≈ 42 GPa.

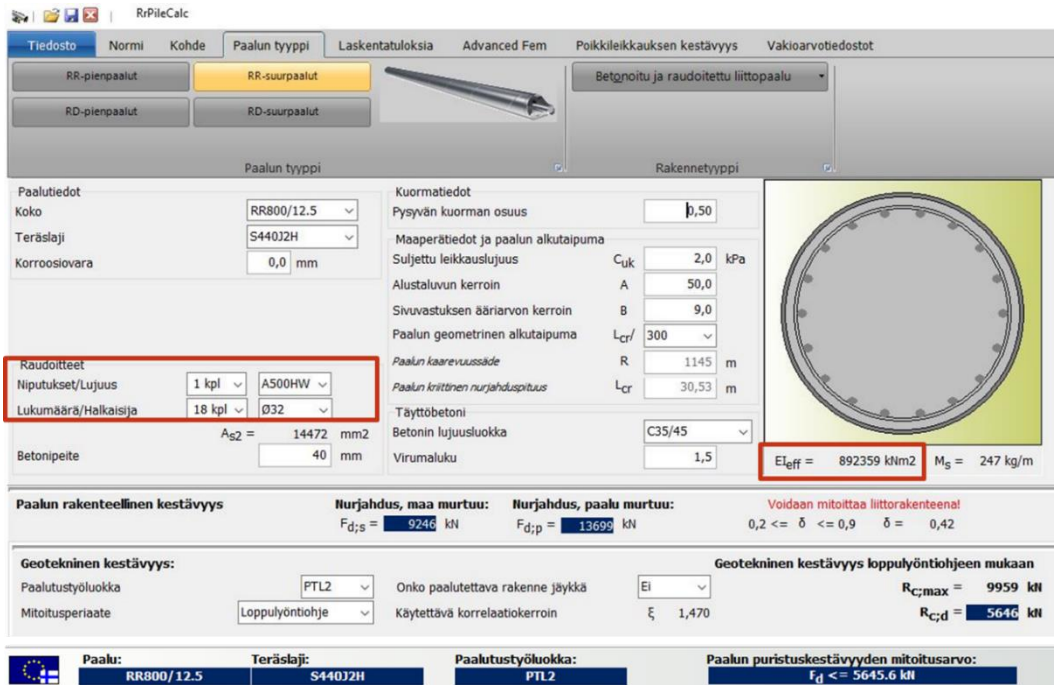

Figure 5-2 Details of RR800/12.5 piles assumed in the analyses. Figure obtained from RrPileCalc software.

Further, dummy beam elements are modelled at the centreline of the piles across the pile length. The reason for using beam elements is to be able to extract pile displacements in a simple way. Such elements are modelled so that the overall pile behaviour (stiffness) is not affected. therefore, a 10^6 times lower stiffness is given to the elastic beam elements.

Input parameters for piles are summarized in Table 5-4.

Table 5-4 Input parameters for piles.

Parameter	**Material type**	**Element type**	**γ**	**E**	**ν**	**D**
Unit			**kN/m³**	**GN/m²**	**-**	**m**
Pile RR800/12.5	Linear Elastic	Volume	28	42	0,3	0,813
Embedded beam (dummy pile)	Elastic	Massive circular beam	$1x10^{-3}$	$42x10^{-6}$	0,3	0,813

6 Results

6.1 Model performance and behaviour

Figure 6-1 and Figure 6-2 show examples of total (σ_{yy}) and effective (σ'_{yy}) stress distribution under the traffic load, respectively, at a longitudinal section taken at x=2,5m through the centreline of the pile for the NCA case with crushed rock embankment, clay subsoil and fixed pile head (NCA-01-S1-T).

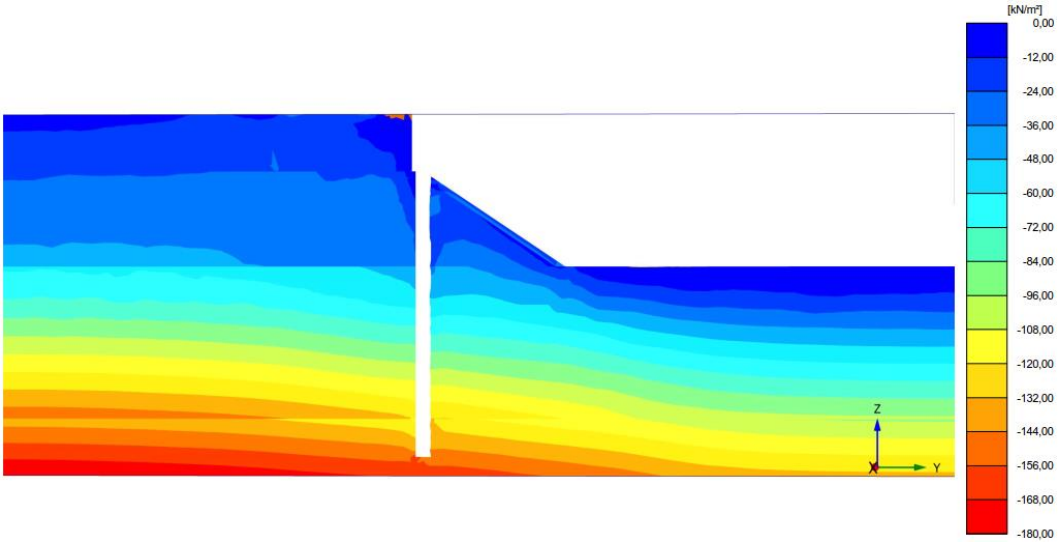

Figure 6-1 Cartesian total stress σ_{yy} – longitudinal section @x=2,5m through the centreline of the pile – NCA-01-S1-T.

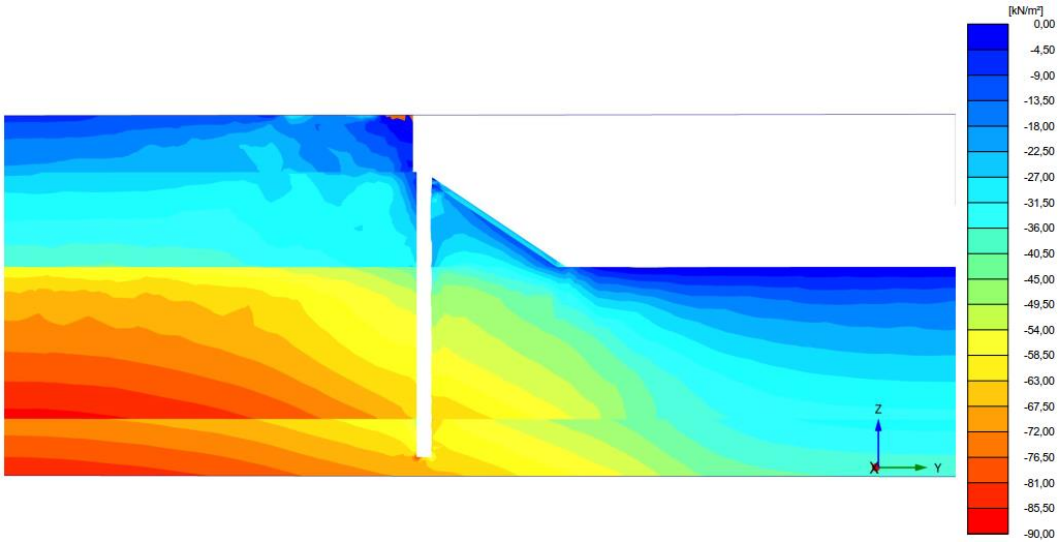

Figure 6-2 Cartesian effective stress σ'_{yy} – longitudinal section @x=2,5m through the centreline of the pile - NCA-01-S1-T.

Figure 6-3 and Figure 6-4 show examples of total displacements for NCA-01-S1-T (sand subsoil) and NCA-01-C1-T, respectively, under the traffic load at the same longitudinal section. It can be noted that the traffic load produces a maximum displacement at surface (settlement) of ≈3-4mm. According to Väylävirasto, this is in line with what is typically observed and somewhat validates the stiffness of the FE model. Further, displacements under the LM-71 loads are ≈4mm for the case with sand subsoil and ≈6,5mm for the case with clay subsoil. Similar values were found in all the other NCA and CA cases analysed. The computed displacements were found to be substantially independent of the FE mesh used.

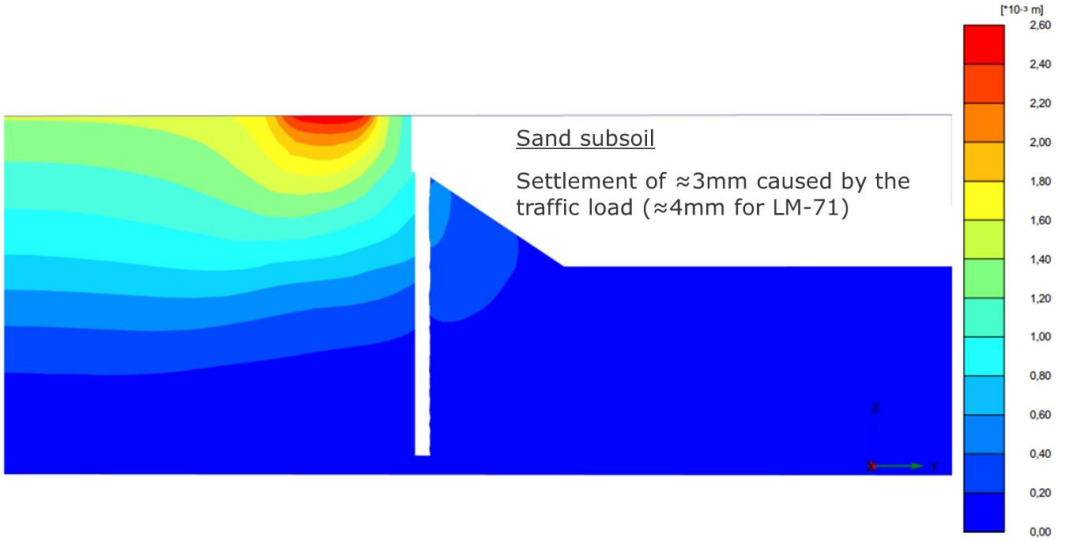

Figure 6-3 Phase displacement - Load application (Phase 2b) – longitudinal section @x=2,5m through the centreline of the pile – NCA-01-S1-T.

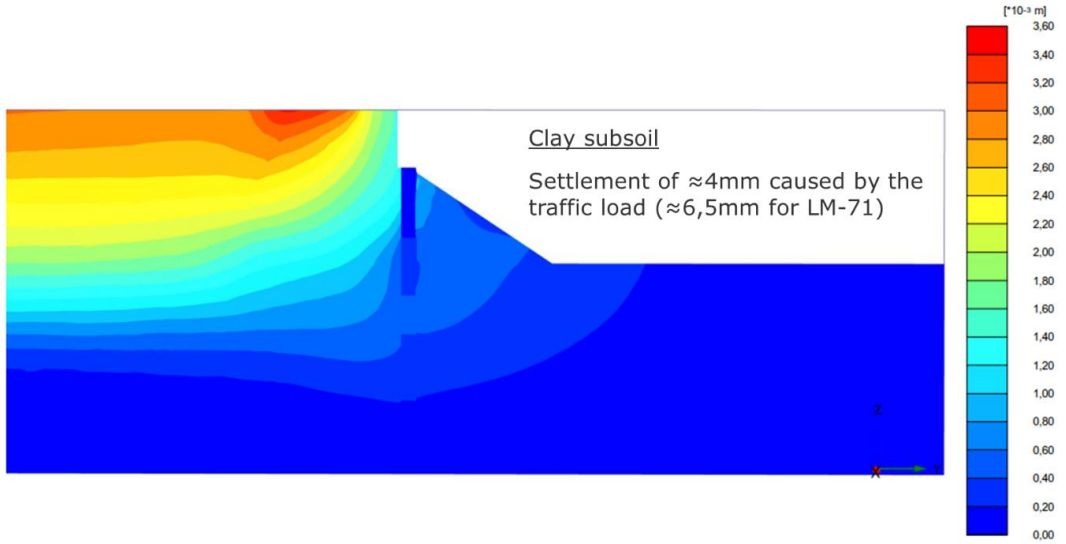

Figure 6-4 Phase displacement - Load application (Phase 2b) – longitudinal section @x=2,5m through the centreline of the pile – NCA-01-C1-T.

6.2 Mesh sensitivity check

The sensitivity of FE results to the element discretization is checked for the pile horizontal displacement under the traffic load. As shown in Figure 6-5, the use of a Very Fine mesh, consisting of approximately 130 000 elements, does not show a significant increase of displacements (less than 1%) compared to the Very Coarse (≈ 19 000 elements) and Medium (≈ 35 000 elements) mesh types. This is true for both CA and NCA configurations and for both clay and sand subsoil. Further, the use of a Very fine mesh increases significantly the computation time. Therefore, the Medium mesh is used in subsequent analyses.

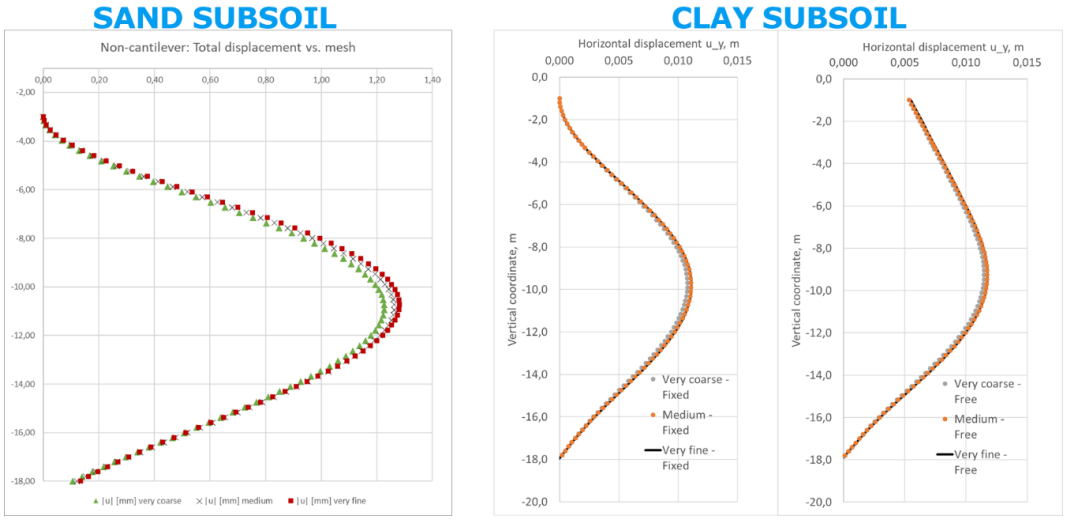

Figure 6-5 Sensitivity of pile displacements to the FE mesh.

6.3 Effect of traffic load configuration

The impact of load traffic asymmetry is checked in Figure 6-6 by comparing pile displacement of the reference pile for different load configurations, i.e. by changing the location of the maximum load (40 kPa over 3m x 5m). The differences in terms of displacements of the reference pile are less than 1%. As expected, the pile displacement increases more significantly when a load of 40 kPa is applied to the whole loading area.

As shown in Figure 6-6, the location of the maximum load does not have any notable effect on pile behaviour. Such a conclusion is anticipated to be valid for all NCA and CA cases and regardless of the subsoil and/or embankment material. Therefore, the "load on right" configuration is taken as the base case configuration to model earth pressure under traffic load.

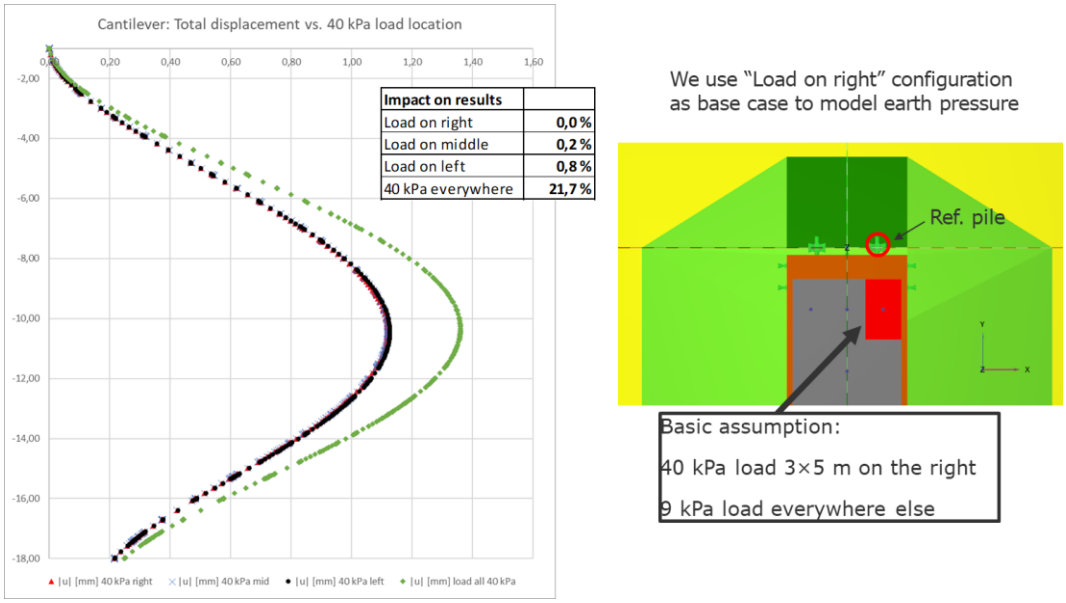

Figure 6-6 Effect of traffic load configuration on pile displacements (NCA-01-S1-T).

6.4 Earth pressure: FEM vs analytical solution

Figure 6-7 to Figure 6-19 show a comparison between the computed earth pressure under traffic and LM-71 loads and the analytical solutions for P1 and P2. **The analytical curves do not include the assumed multiplying factor of 3 that accounts for gathering of earth pressure from an area equal to 3 times the pile diameter (see section 0).** The two analysed LM-71 load configurations (distributed and bogies) give substantially similar results, as shown in Figure 6-7 and Figure 6-8. Therefore, only the "52 kPa + 27 kPa" LM-71 load results are presented in Figure 6-9 to Figure 6-19 together with the "9 kPa + 31 kPa" traffic load.

In the analytical solution for P2, average traffic/train loads are selected to model P and P2 in equations (3) and (4). In detail, P = 10 kPa with B = 10 m and P = 32 kPa with B = 7,5 m are selected for traffic load and LM-71 load, respectively.

In most cases, the analytical solution appears to deviate from the FE results. In particular, it severely underestimates the earth pressure in undrained conditions. The analytical solution seems to be more in line with the earth pressure in the coarse layers when the model is governed by drained conditions (i.e. sand subsoil). Nevertheless, the solution is based on K_o conditions and it only accounts for the K_o of the superstructure. On the other hand, the mobilized earth pressure may deviate from K_o conditions according to the degree of mobilization.

In undrained conditions, the two solutions show a discrepancy even in the coarse layers, especially for the NCA cases with clay subsoil (see Figure 6-17 and Figure 6-19). One possible reason may be the high shear mobilization in the embankment that results from the simulation of long-term conditions (large settlement after construction). In this way, the embankment and superstructure will show a softer behaviour compared to the case with sand subsoil, with consequent stress concentration and earth pressure increase behind the fixed

piles. This behaviour seems to be less pronounced in the CA model with fixed pile head (Figure 6-10 and Figure 6-14), while it tends to disappear when the pile head is free to move (Figure 6-11 and Figure 6-15). It must be noted that the distance between the centre of the pile and the abutment wall is larger in the CA model (2,5m) compared to the NCA model (0,6m).

1) CA-01-S1-T

- Traffic load 9 kPa + 31 kPa

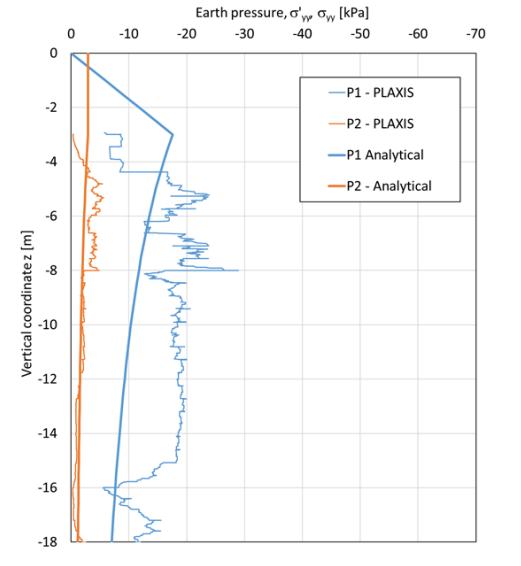

2) CA-01-S1-R1

- LM-71 load 52 kPa + 27 kPa

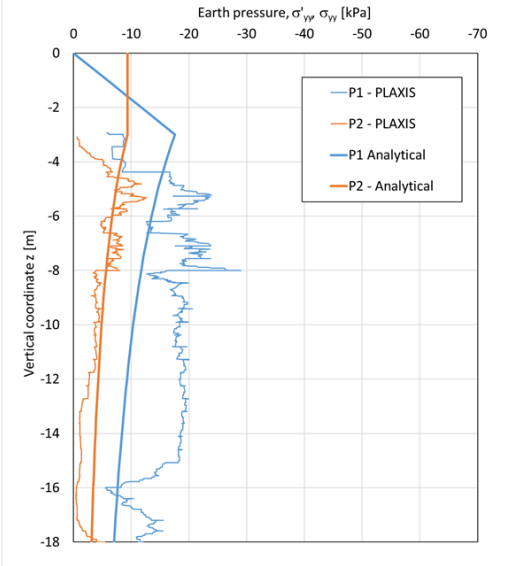

Figure 6-7 FE vs analytical earth pressure solution for CA-01-S1-T and CA-01-S1-R1 (embankment: crushed rock; subsoil: sand; pile head: fixed)

3) CA-01-S1-R2

- LM-71 load 52 kPa + 52 kPa

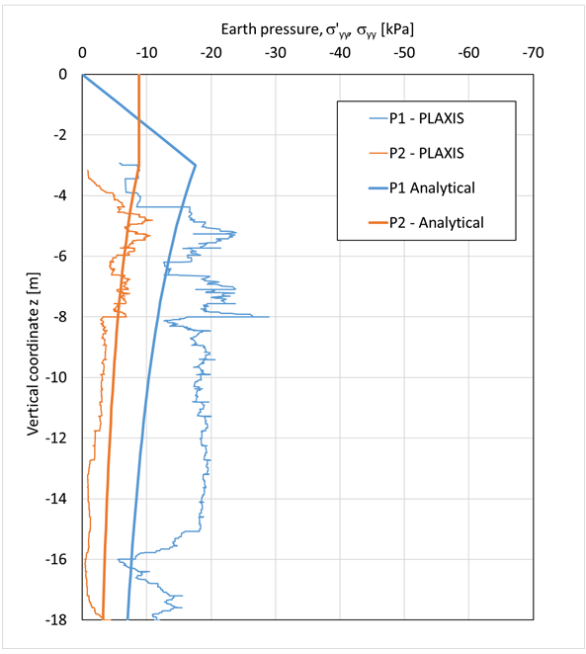

Figure 6-8 FE vs analytical earth pressure solution for CA-01-S1-R2 (embankment: crushed rock; subsoil: sand; pile head: fixed)

4) CA-01-S2-T

- Traffic load 9 kPa + 31 kPa

5) CA-01-S2-R1

- LM-71 load 52 kPa + 27 kPa

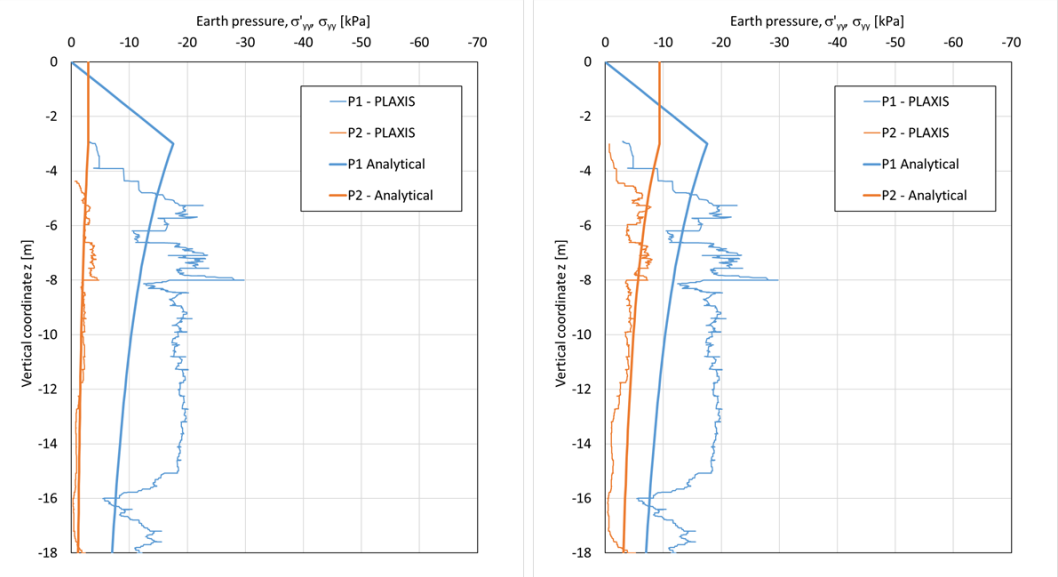

Figure 6-9 FE vs analytical earth pressure solution for CA-01-S2-T and CA-01-S2-R1 (embankment: crushed rock; subsoil: sand; pile head: free)

7) CA-01-C1-T

- Traffic load 9 kPa + 31 kPa

8) CA-01-C1-R1

- LM-71 load 52 kPa + 27 kPa

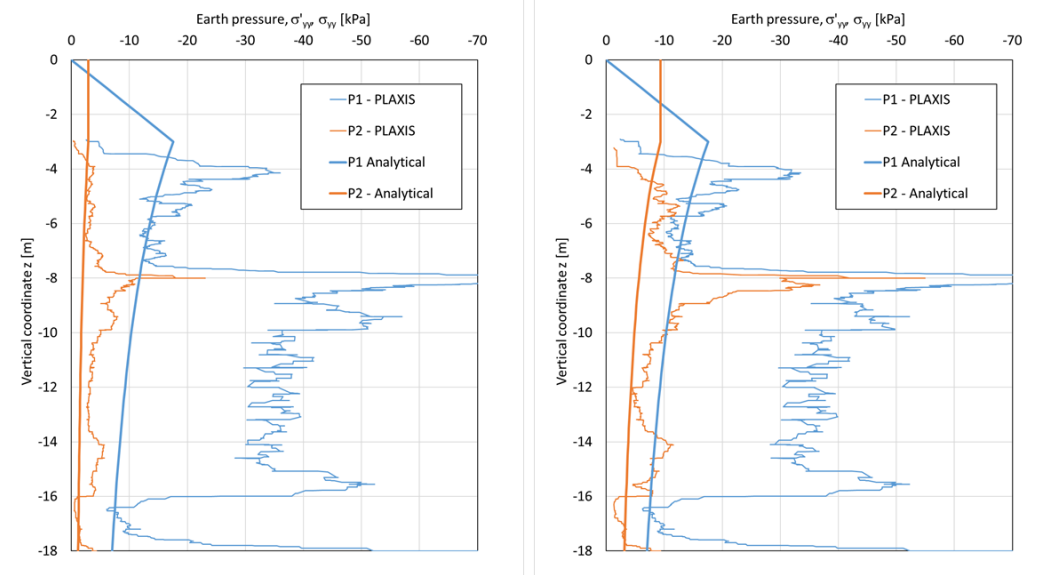

Figure 6-10 FE vs analytical earth pressure solution for CA-01-C1-T and CA-01-C1-R1 (embankment: crushed rock; subsoil: clay; pile head: fixed)

10) CA-01-C2-T

- Traffic load 9 kPa + 31 kPa

11) CA-01-C2-R1

- LM-71 load 52 kPa + 27 kPa

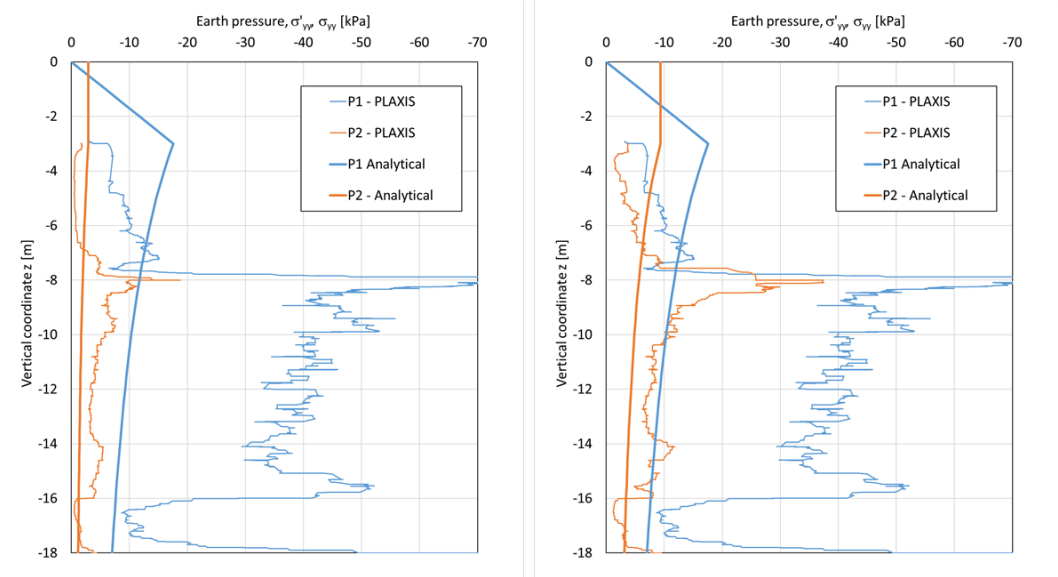

Figure 6-11 FE vs analytical earth pressure solution for CA-01-C2-T and CA-01-C2-R1 (embankment: crushed rock; subsoil: clay; pile head: free)

13) CA-02-S1-T

- Traffic load 9 kPa + 31 kPa

14) CA-02-S1-R1

- LM-71 load 52 kPa + 27 kPa

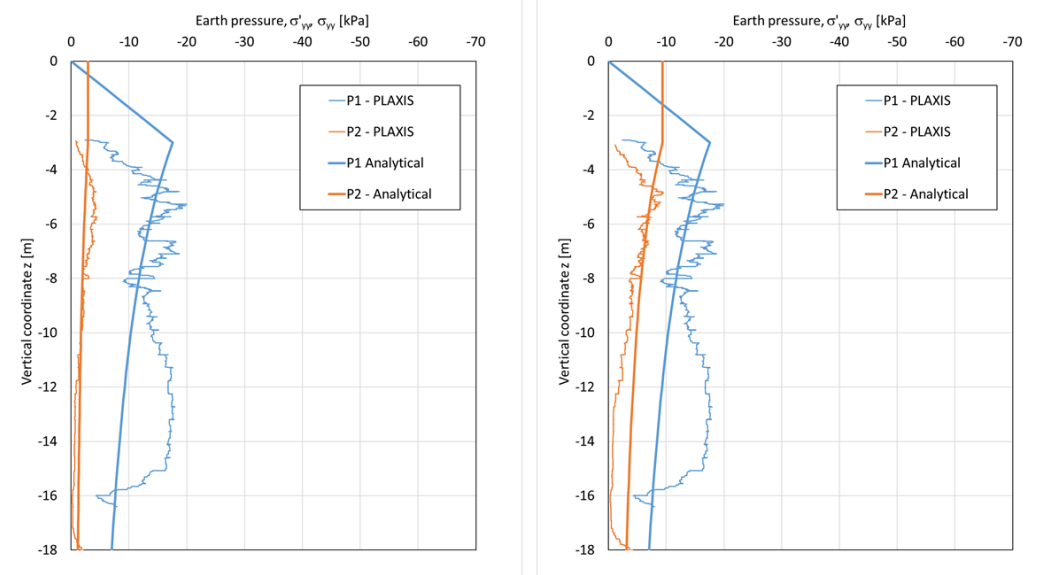

Figure 6-12 FE vs analytical earth pressure solution for CA-02-S1-T and CA-02-S1-R1 (embankment: sand; subsoil: sand; pile head: fixed)

16) CA-02-S2-T

- Traffic load 9 kPa + 31 kPa

17) CA-02-S2-R1

- LM-71 load 52 kPa + 27 kPa

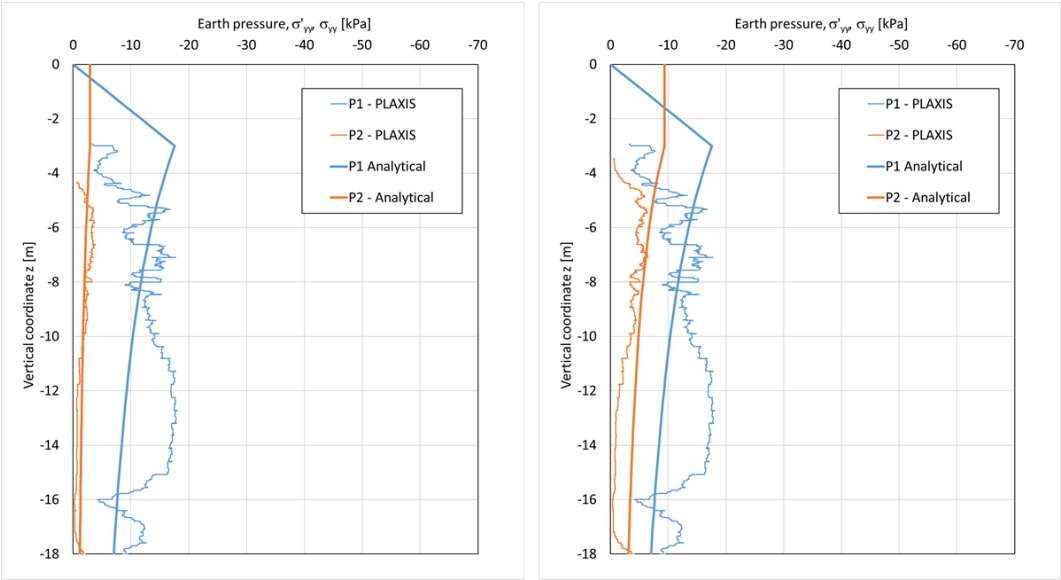

Figure 6-13 FE vs analytical earth pressure solution for CA-02-S2-T and CA-02-S2-R1 (embankment: sand; subsoil: sand; pile head: free)

19) CA-02-C1-T

- Traffic load 9 kPa + 31 kPa

20) CA-02-C1-R1

- LM-71 load 52 kPa + 27 kPa

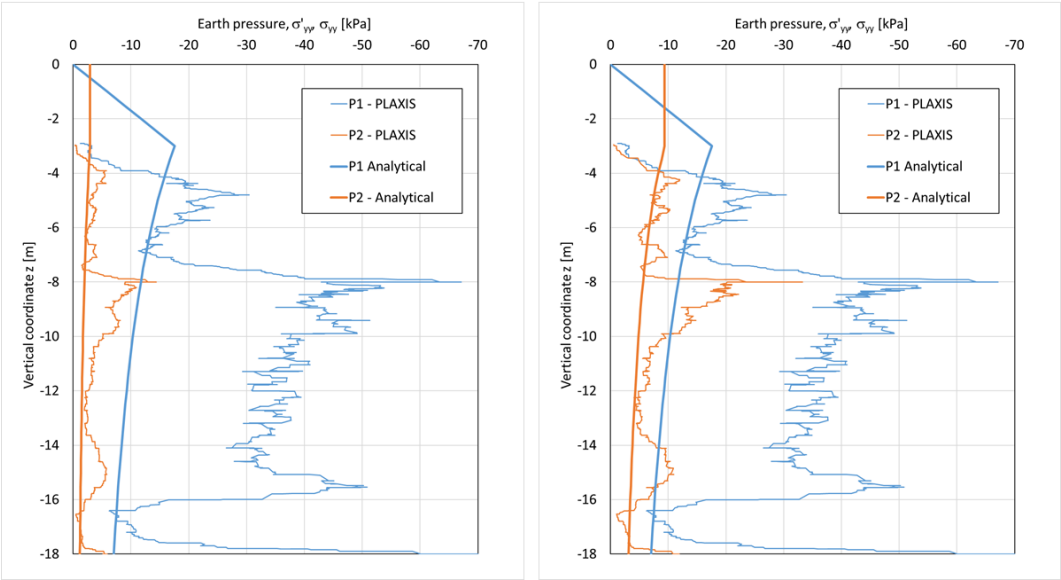

Figure 6-14 FE vs analytical earth pressure solution for CA-02-C1-T and CA-02-C1-R1 (embankment: sand; subsoil: clay; pile head: fixed)

22) CA-02-C2-T

- Traffic load 9 kPa + 31 kPa

23) CA-02-C2-R1

- LM-71 load 52 kPa + 27 kPa

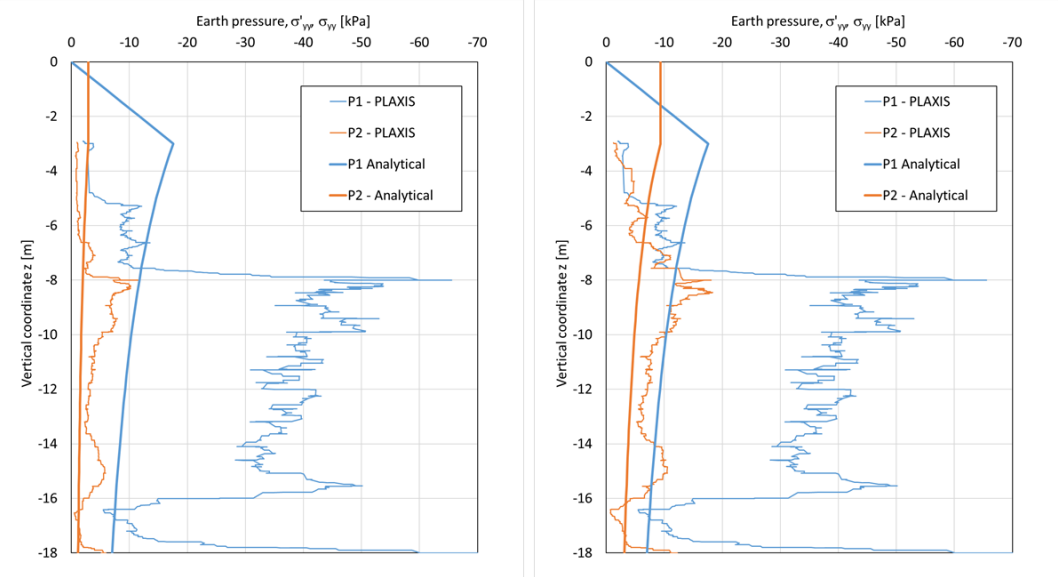

Figure 6-15 FE vs analytical earth pressure solution for CA-02-C2-T and CA-02-C2-R1 (embankment: sand; subsoil: clay; pile head: free)

25) NCA-01-S1-T

- Traffic load 9 kPa + 31 kPa

26) NCA-01-S1-R1

- LM-71 load 52 kPa + 27 kPa

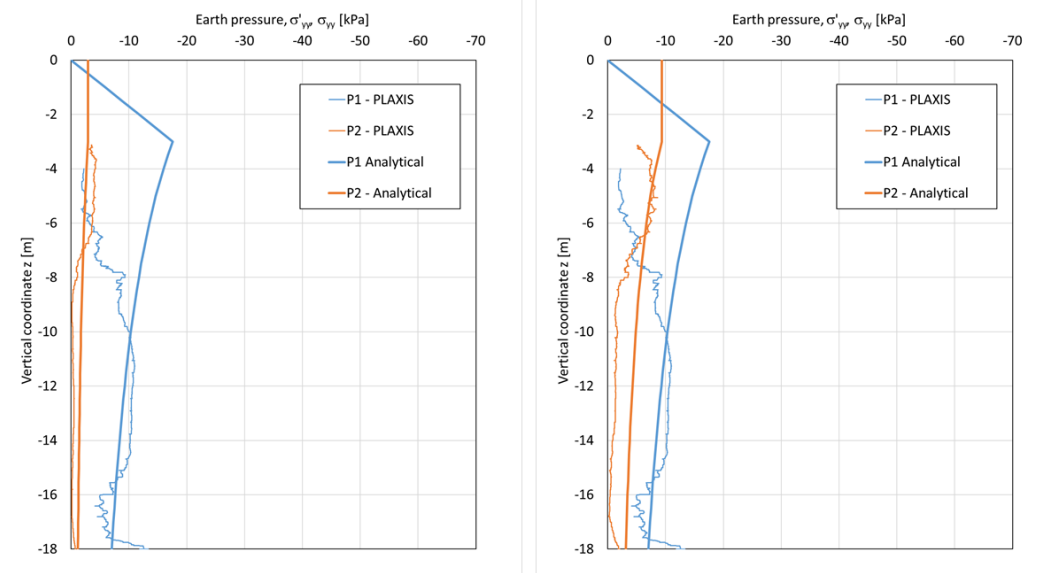

Figure 6-16 FE vs analytical earth pressure solution for NCA-01-S1-T and NCA-01-S1-R1 (embankment: crushed rock; subsoil: sand; pile head: fixed)

28) NCA-01-C1-T

- Traffic load 9 kPa + 31 kPa

29) NCA-01-C1-R1

- LM-71 load 52 kPa + 27 kPa

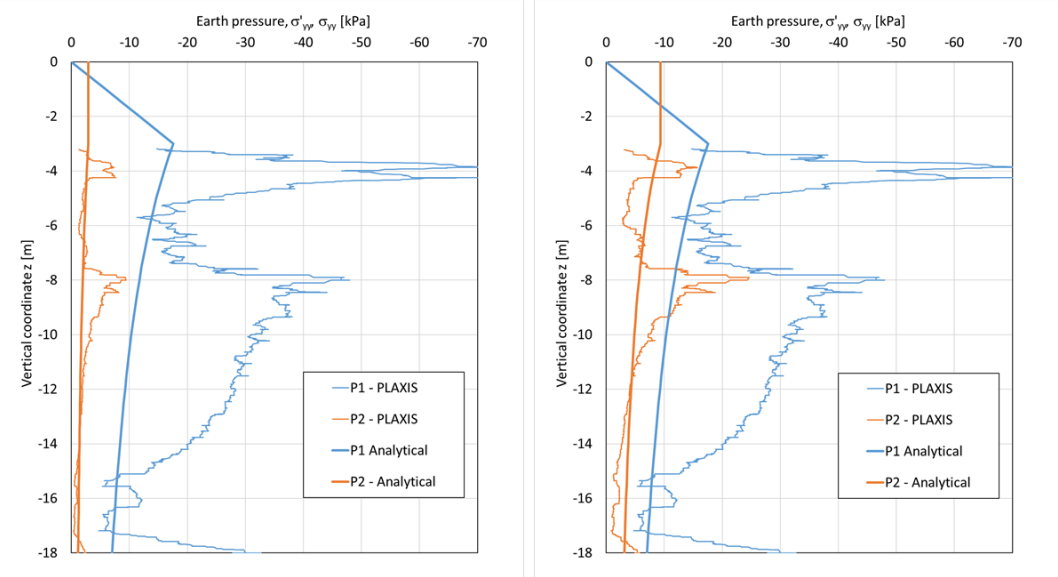

Figure 6-17 FE vs analytical earth pressure solution for NCA-01-C1-T and NCA-01-C1-R1 (embankment: crushed rock; subsoil: clay; pile head: fixed)

31) NCA-02-S1-T

- Traffic load 9 kPa + 31 kPa

32) NCA-02-S1-R1

- LM-71 load 52 kPa + 27 kPa

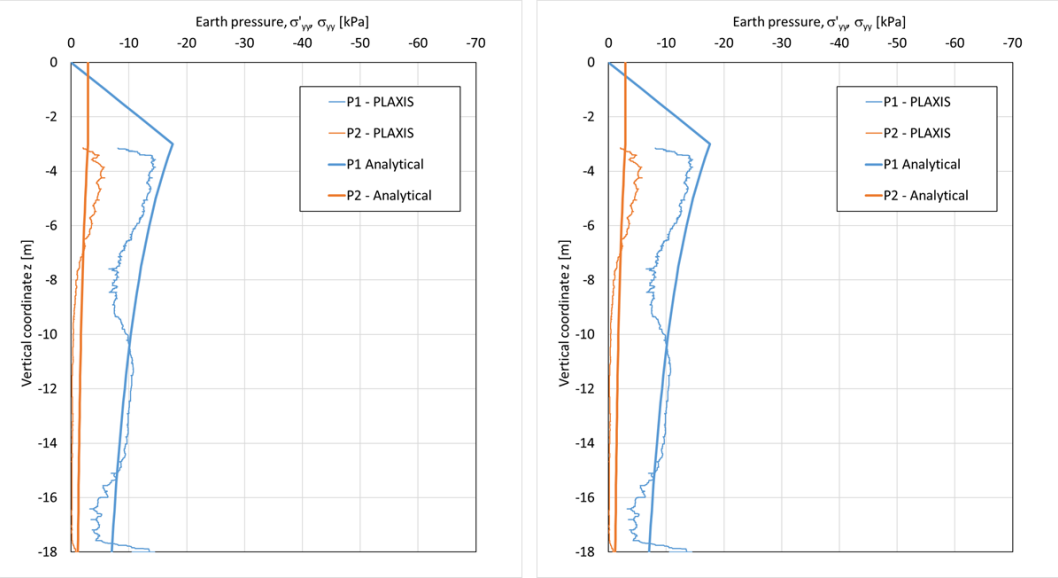

Figure 6-18 FE vs analytical earth pressure solution for NCA-02-S1-T and NCA-02-S1-R1 (embankment: sand; subsoil: sand; pile head: fixed)

34) NCA-02-C1-T

- Traffic load 9 kPa + 31 kPa

35) NCA-02-C1-R1

- LM-71 load 52 kPa + 27 kPa

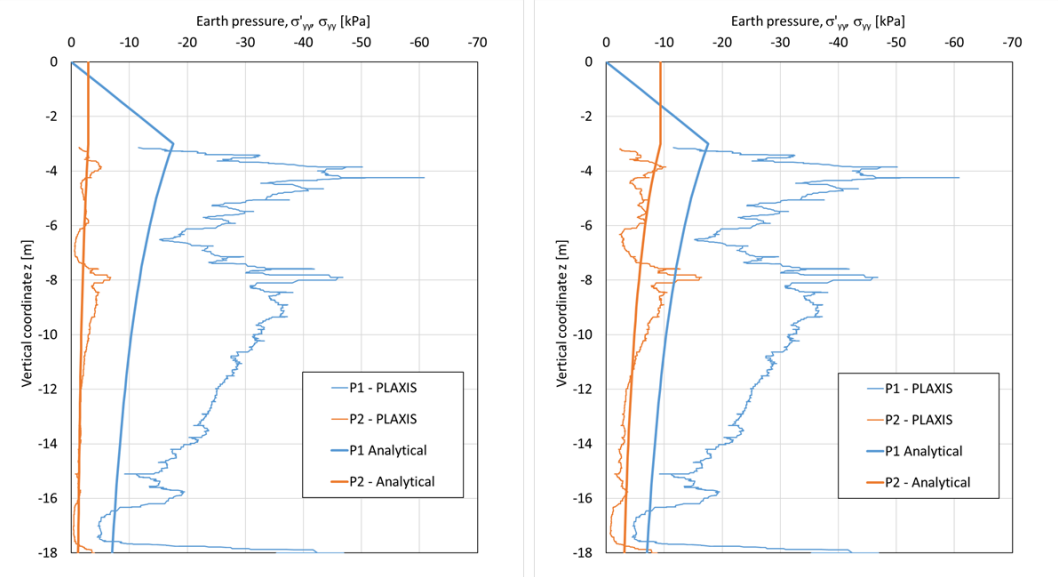

Figure 6-19 FE vs analytical earth pressure solution for NCA-02-C1-T and NCA-02-C1-R1 (embankment: sand; subsoil: clay; pile head: fixed)

6.5 Earth pressure on active vs passive side

The earth pressures acting behind and in front of the piles are compared for some relevant cases (Figure 6-20 to Figure 6-22). For simplicity, these earth pressures are referred to as "Active" and "Passive", even though they do not refer to ultimate active and passive failure states (they represent mobilized values that result in equilibrium of the pile system). The passive earth pressure is modelled following the method presented in section 4.4, with the difference that the representative cross section is taken right in front of the pile.

Results show that discrepancies exist between earth pressures acting on the two sides of the piles. In general, the active earth pressure is larger than the passive one, especially for the situations where the pile head is fixed, and the subsoil is clay (CA in Figure 6-20, NCA in Figure 6-22). Such differences appear to be less significant in presence of sandy subsoil. When the pile head is modelled as free, the mobilized passive resistance appears to be larger than the active one, especially in the proximity of the pile head. This effect is clearly visible especially when the subsoil is clay (CA in Figure 6-21).

The reason why the mobilized active earth pressure is higher than the mobilized passive pressure can be explained by force equilibrium. If the horizontal force equilibrium of a pile is considered, the active and passive resulting forces need to be equal. A considerable passive force is provided by the pile head (when it is fixed), so less passive earth pressure is mobilized to maintain overall horizontal equilibrium. For the free pile head case this does not apply. In the case of free pile head in clay subsoil, the passive earth pressure needed for equilibrium is mobilized in the embankment.

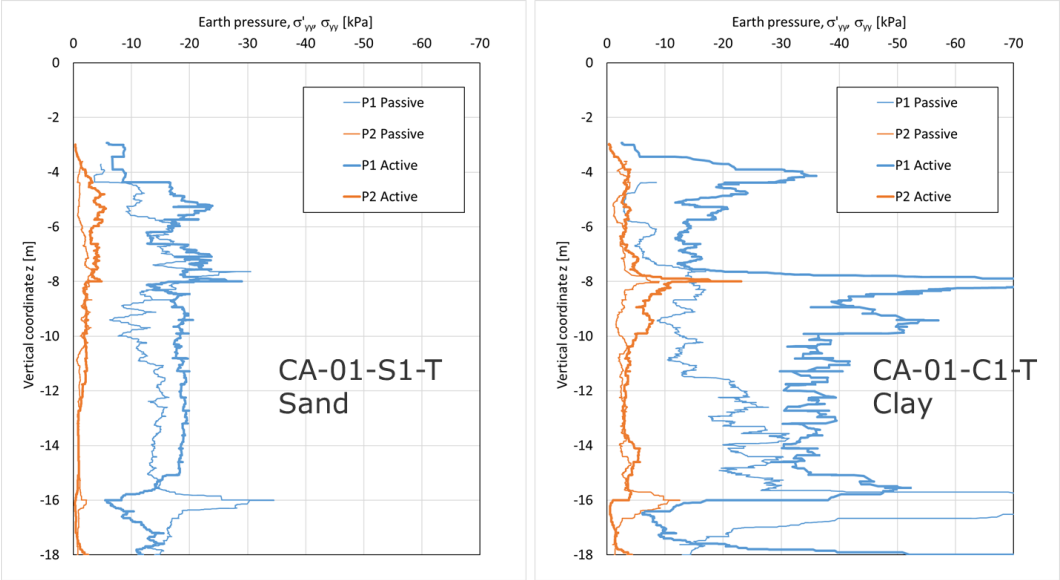

Figure 6-20 Comparison of calculated active vs passive earth pressures on piles for CA-01-S1-T and CA-01-C1-T (embankment: crushed rock; subsoil: sand/clay; pile head: fixed).

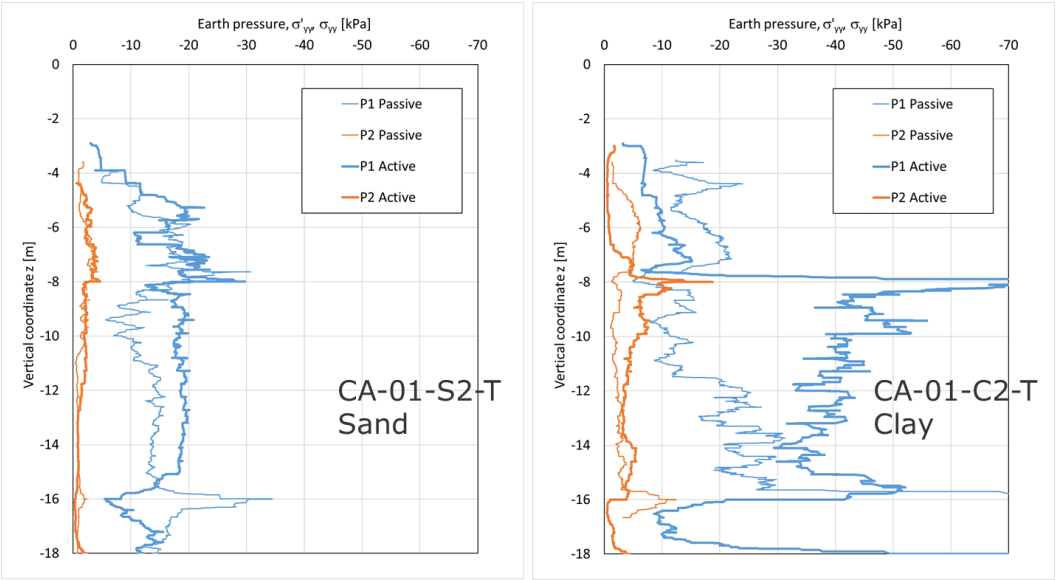

Figure 6-21 Comparison of calculated active vs passive earth pressures on piles for CA-01-S2-T and CA-01-C2-T (embankment: crushed rock; subsoil: sand/clay; pile head: free).

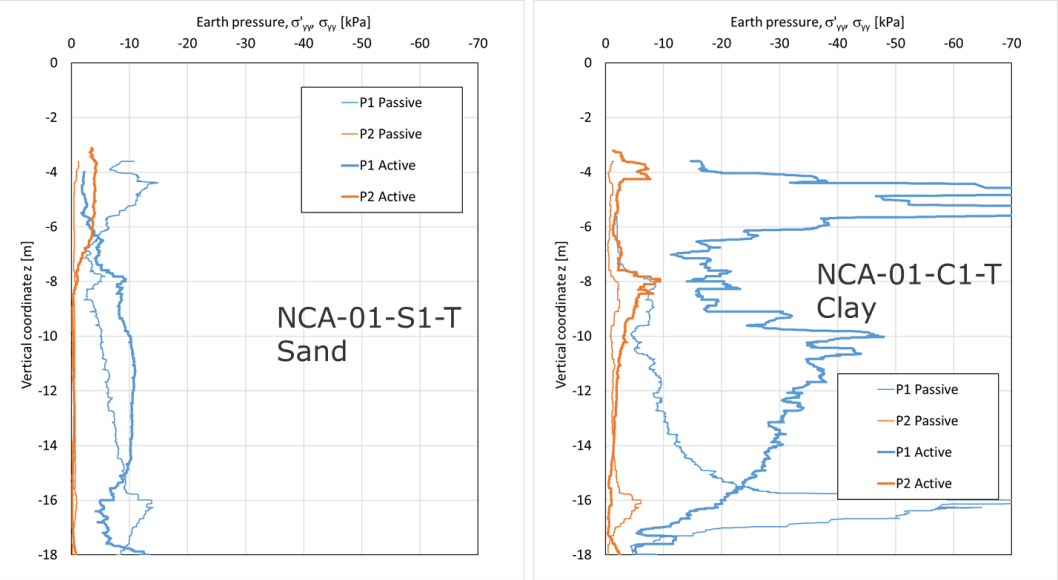

Figure 6-22 Comparison of calculated active vs passive earth pressures on piles for NCA-01-S1-T and NCA-01-C1-T (embankment: crushed rock; subsoil: sand/clay; pile head: fixed).

6.6 Pile displacements

Figure 6-23 illustrates the computed horizontal pile displacement (u_y) from the combined superstructure and traffic load for the different NCA and CA models. For the CA cases with sand subsoil, $u_{y\_max} \approx$ 1,5-2,5 mm; while in presence of clay subsoil $u_{y\_max} \approx$ 6,5-7,5 mm. For the NCA cases with sand subsoil, $u_{y\_max} \approx$ 1-1,3 mm; while in presence of clay subsoil $u_{y\_max} \approx$ 5,5-6 mm.

In general, u_y in clay is about 5-6 times than u_y in sand. The maximum calculated horizontal pile head displacement is 5,5 mm and is obtained from the CA case with sand embankment and clay subsoil.

Figure 6-24 compares u_y under traffic and LM-71 loads for the CA models with crushed rock embankments and clay subsoil. The value of u_{y_max} increases by ≈1 mm under the LM-71 load. Similar results are obtained for all the other CA and NCA models.

Figure 6-25 to Figure 6-30 show u_y from the different calculation phases. The sole traffic load phase generates a displacement of less than 1 mm. Most of the deformations and, hence, earth pressure, appear to derive from the superstructure construction phase.

In conclusion, traffic (road or railway) loading seems to cause approximately 10% of the total pile movement when the pile head is modelled as fixed; while it causes approximately 15-20% of the total pile movement in the upper part of the pile with free head.

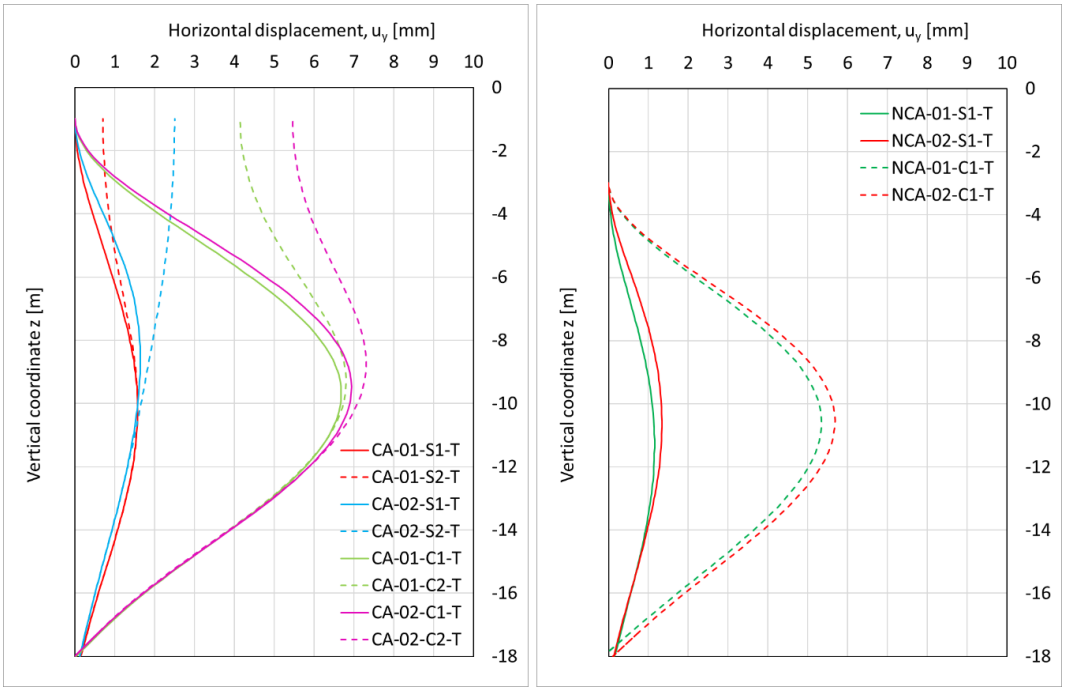

Figure 6-23 Horizontal pile displacement under traffic load for NCA and CA models (embankment: crushed rock/sand; subsoil: sand/clay; pile head: fixed/free)

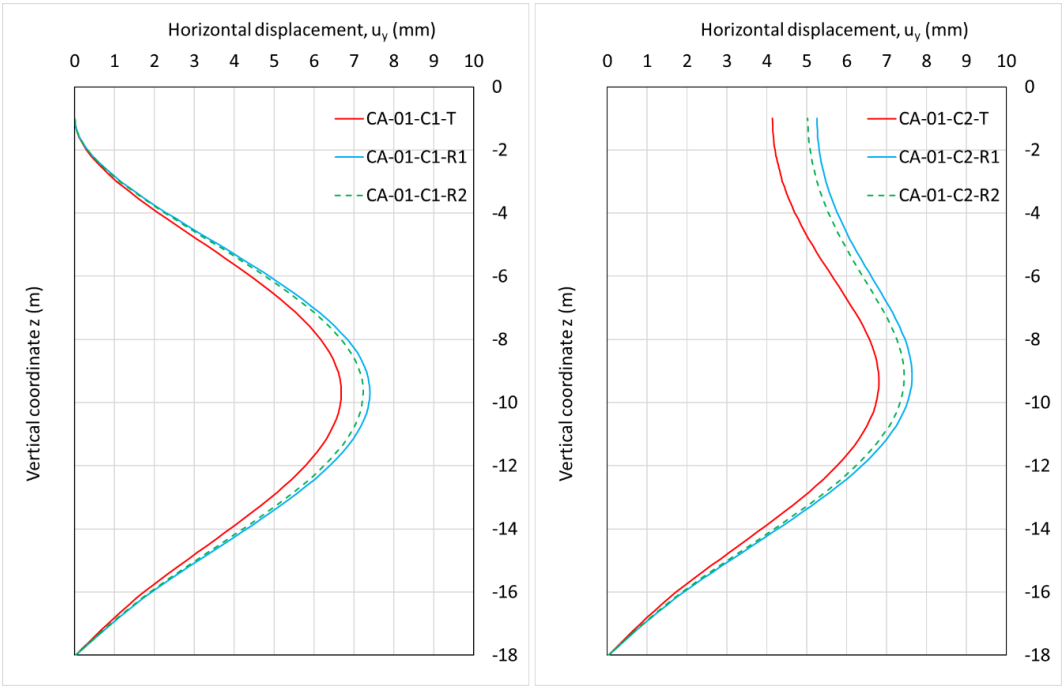

Figure 6-24 Horizontal pile displacement: comparison between traffic load and LM-71 loads from CA-01-C1-T, CA-01-C1-R1 and CA-01-C1-R2 (embankment: sand; subsoil: sand/clay; pile head: fixed/free)

1) CA-01-S1-T

- Traffic load 9 kPa + 31 kPa

7) CA-01-C1-T

- Traffic load 9 kPa + 31 kPa

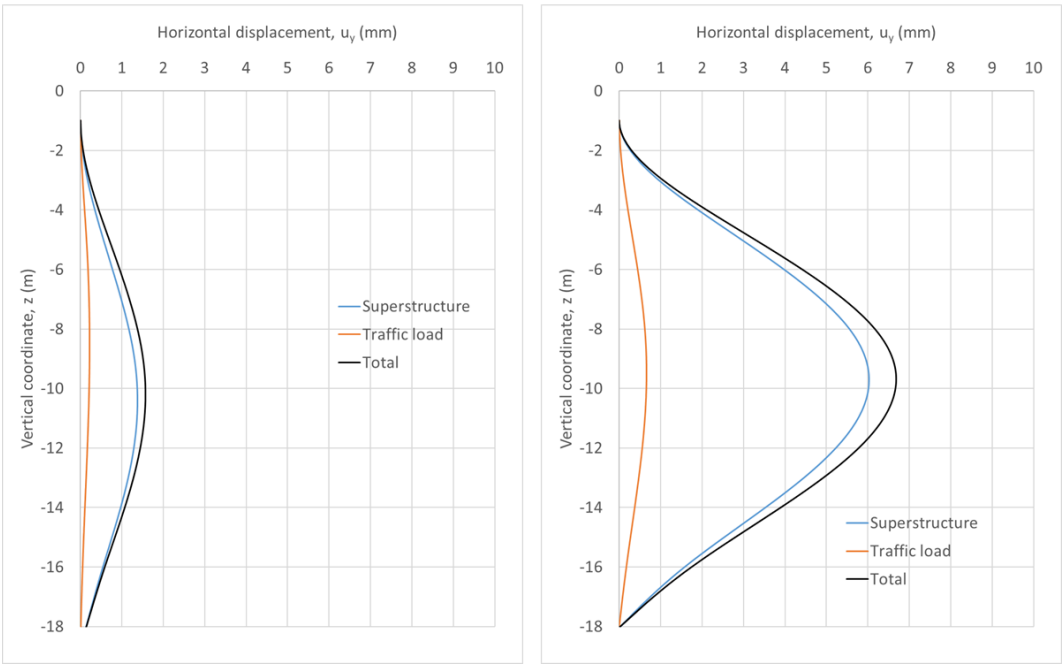

Figure 6-25 Horizontal pile displacement for CA-01-S1-T and CA-01-C1-T under traffic load (embankment: crushed rock; subsoil: sand/clay; pile head: fixed)

4) CA-01-S2-T

- Traffic load 9 kPa + 31 kPa

10) CA-01-C2-T

- Traffic load 9 kPa + 31 kPa

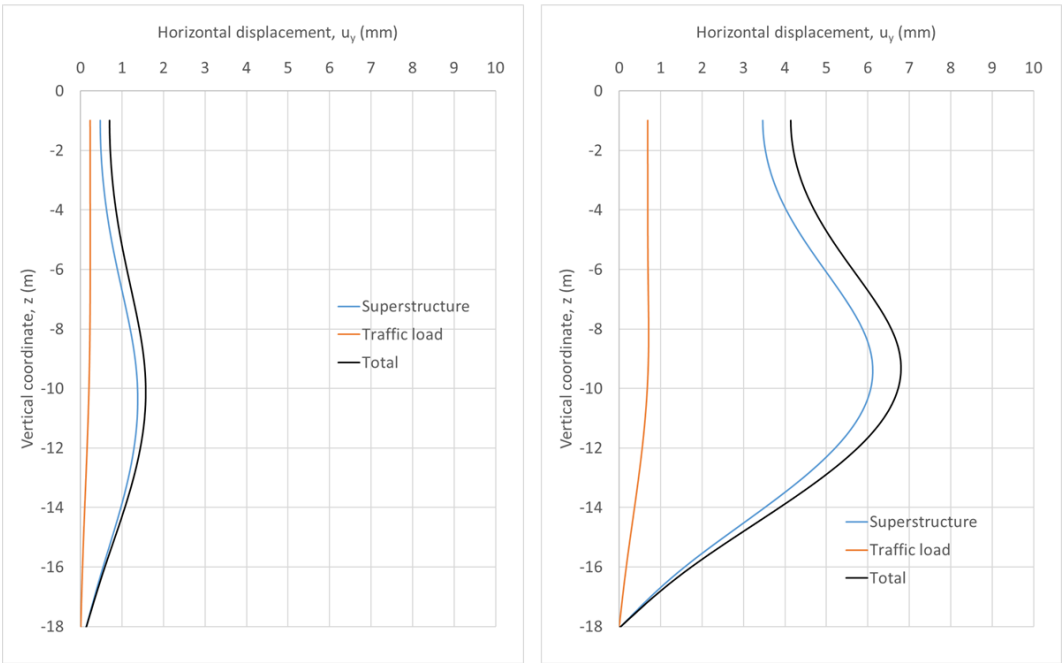

Figure 6-26 Horizontal pile displacement for CA-01-S2-T and CA-01-C2-T under traffic load (embankment: crushed rock; subsoil: sand/clay; pile head: free)

13) CA-02-S1-T

- Traffic load 9 kPa + 31 kPa

19) CA-02-C1-T

- Traffic load 9 kPa + 31 kPa

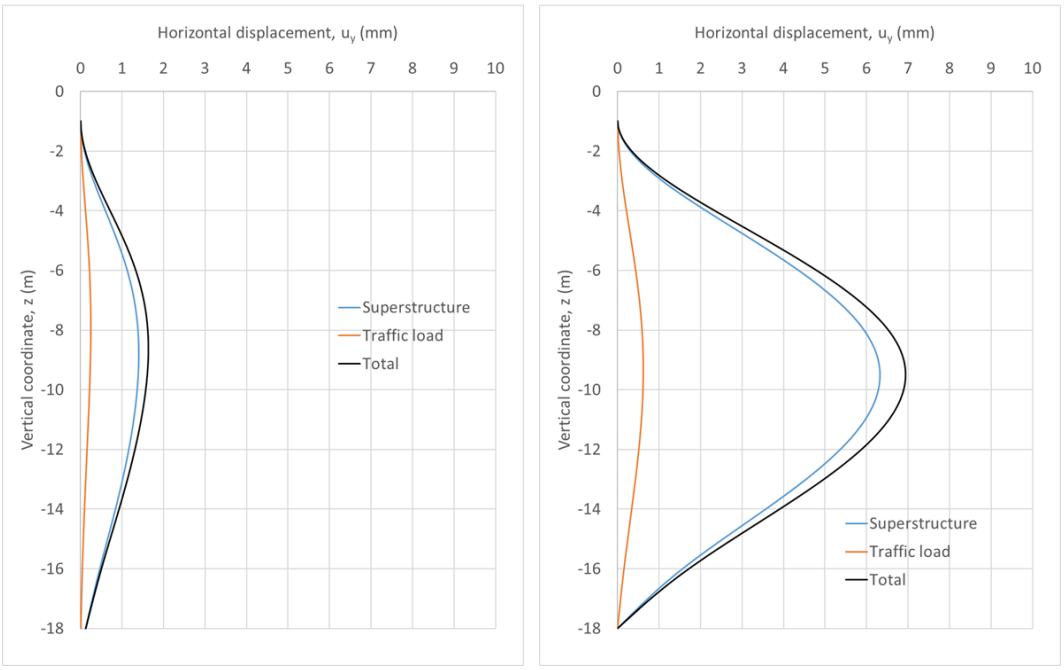

Figure 6-27 Horizontal pile displacement for CA-02-S1-T and CA-02-C1-T under traffic load (embankment: sand; subsoil: sand/clay; pile head: fixed)

16) CA-02-S2-T

- Traffic load 9 kPa + 31 kPa

22) CA-02-C2-T

- Traffic load 9 kPa + 31 kPa

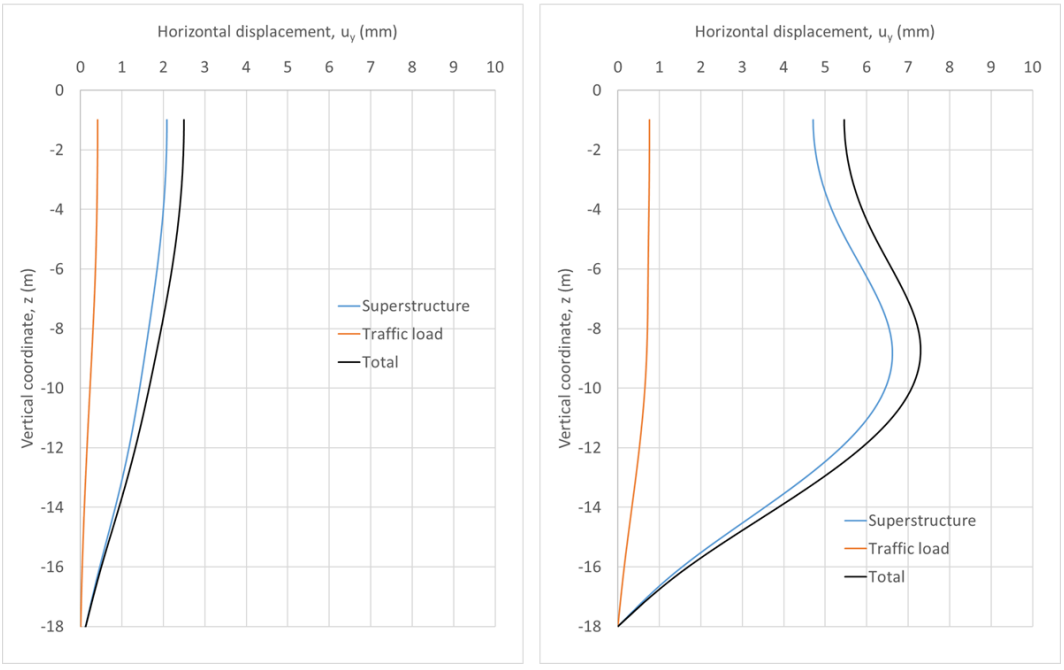

Figure 6-28 Horizontal pile displacement for CA-02-S2-T and CA-02-C2-T under traffic load (embankment: sand; subsoil: sand/clay; pile head: free)

25) NCA-01-S1-T

- Traffic load 9 kPa + 31 kPa

28) NCA-01-C1-T

- Traffic load 9 kPa + 31 kPa

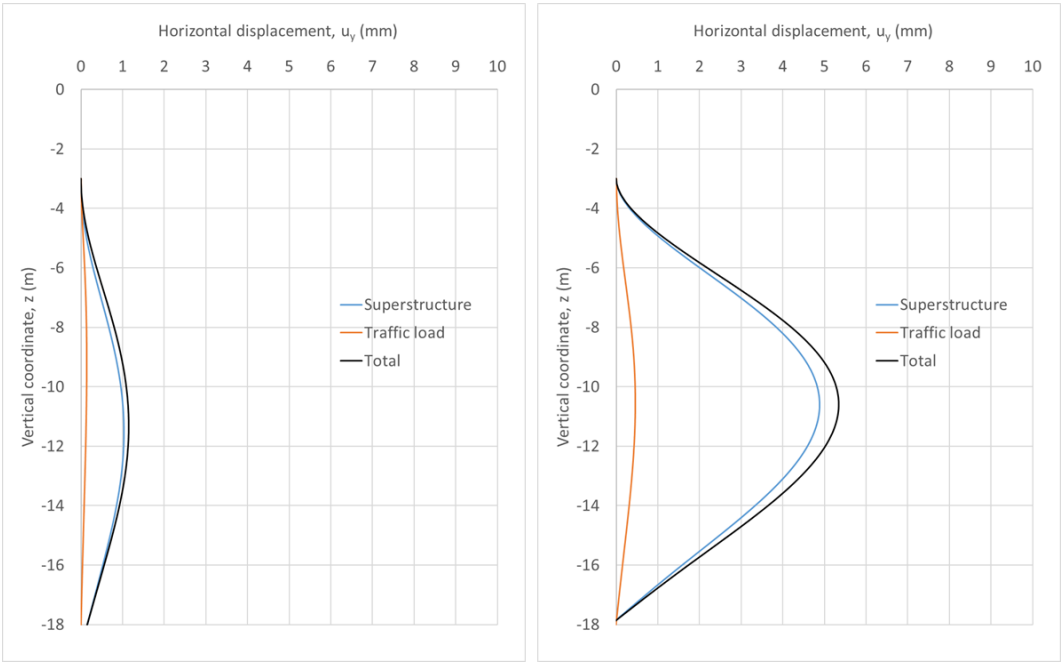

Figure 6-29 Horizontal pile displacement for NCA-01-S1-T and NCA-01-C1-T under traffic load (embankment: crushed rock; subsoil: sand/clay; pile head: fixed)

31) NCA-02-S1-T

- Traffic load 9 kPa + 31 kPa

34) NCA-02-C1-T

- Traffic load 9 kPa + 31 kPa

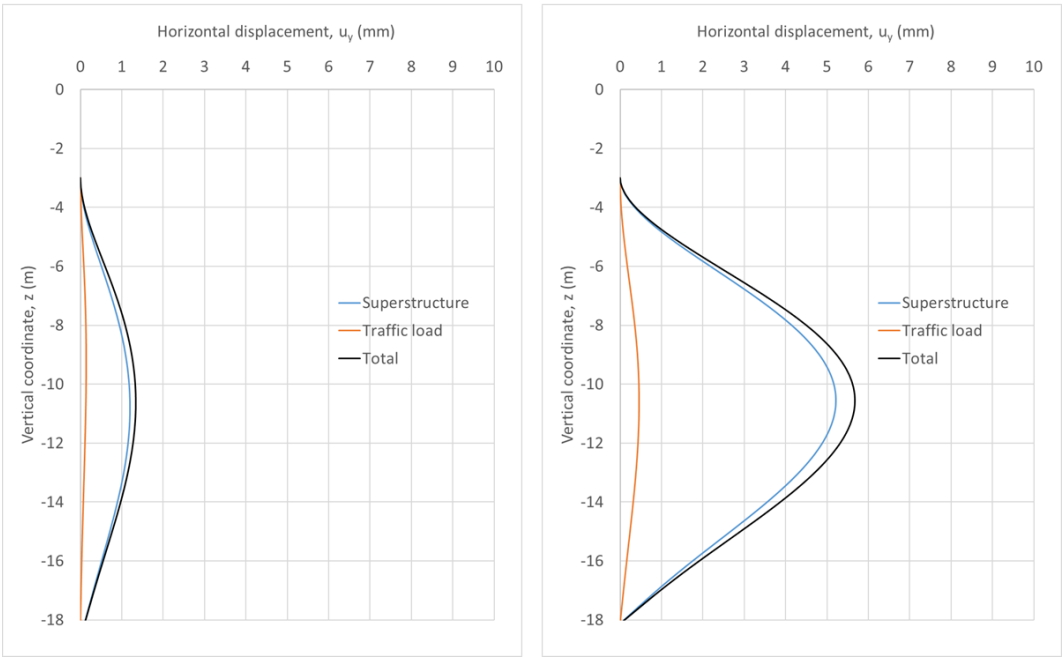

Figure 6-30 Horizontal pile displacement for NCA-02-S1-T and NCA-02-C1-T under traffic load (embankment: sand; subsoil: sand/clay; pile head: fixed)

6.7 Earth pressure distribution

Figure 6-31 to Figure 6-38 show the earth pressure distribution under the traffic load acting on a cross section taken right behind the piles at y=-0,41m. Since the cross section is normal to the y-axis, the normal stress to the surface corresponds to σ'_{yy} (effective) or σ_{yy} (total).

Figure 6-31 and Figure 6-33 suggest a 5-10 kPa difference in the sand subsoil between the earth pressure on the piles and the soil between piles. Such a difference is ≈25 kPa in both crushed rock and sand embankment. Similar results are obtained for the free pile-head configurations and for the LM-71 loads.

Figure 6-32 and Figure 6-34 suggest a ≈25 kPa difference in the clay subsoil between the earth pressure on the piles and the soil between piles. Such a difference is ≈25-50 kPa in the crushed rock and up to ≈25 kPa in the sand embankment. Similar results are obtained for the free pile-head configurations and for the LM-71 loads.

Figure 6-35 and Figure 6-37 suggest a ≈5 kPa difference in the sand subsoil between the earth pressure on the piles and the soil between piles. Such a difference is ≈10 kPa in the crushed rock and ≈0-5 kPa in the sand embankment. Similar results are obtained for the LM-71 loads.

Figure 6-36 and Figure 6-38 suggest a ≈10-30 kPa difference in the clay subsoil between the earth pressure on the piles and the soil between piles. Such a difference is ≈10 kPa in the crushed rock and ≈10-25 kPa in the sand embankment. Similar results are obtained for the LM-71 loads.

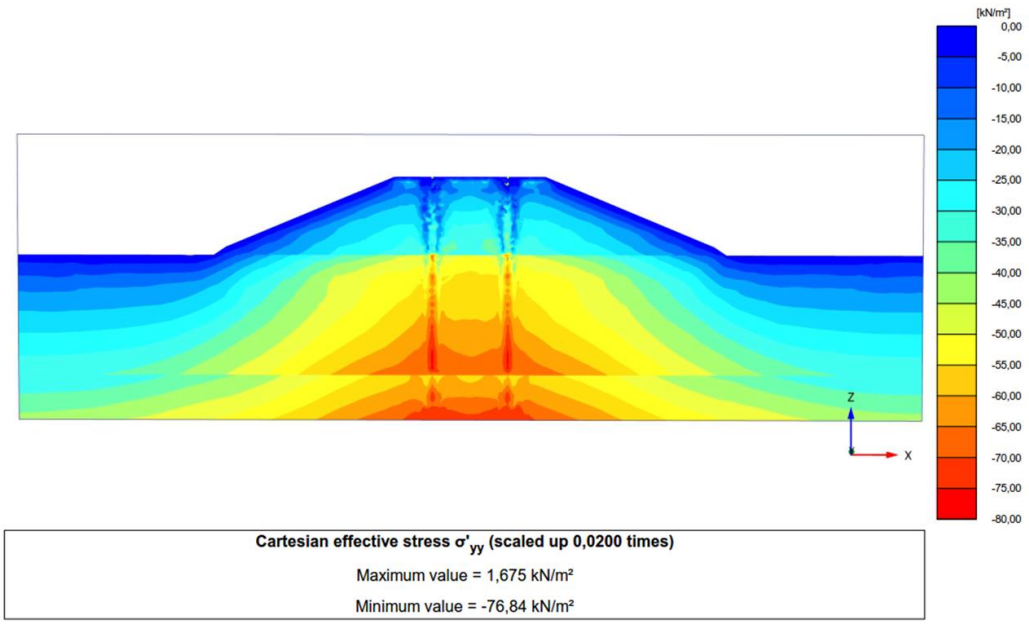

Figure 6-31 Cartesian effective stress σ'_{yy} – cross section @y=0,41m - CA-01-S1-T (embankment: crushed rock; subsoil: sand; pile head: fixed)

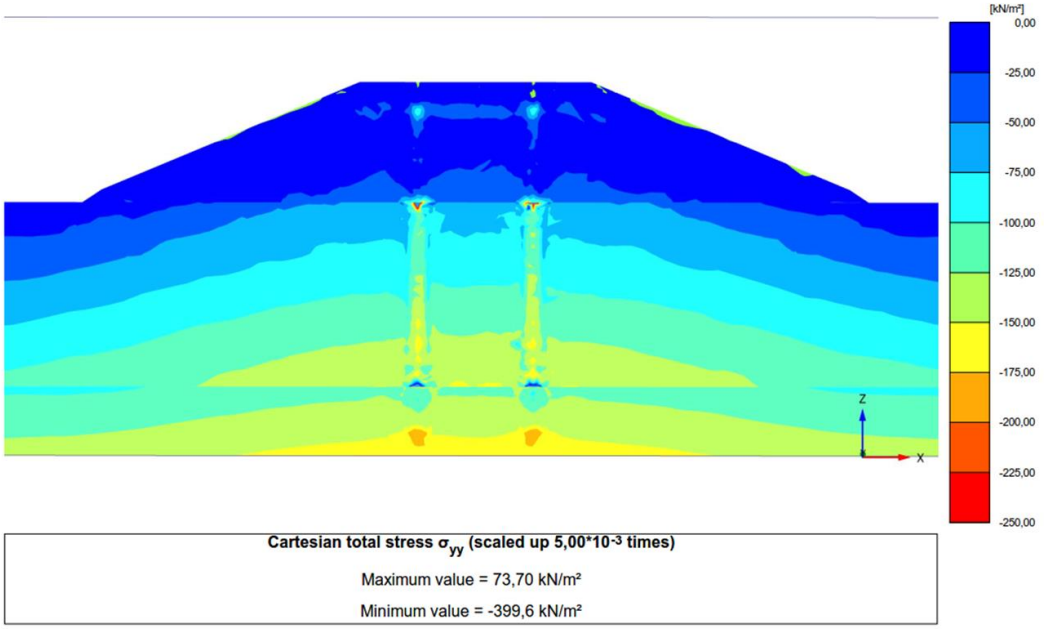

Figure 6-32 Cartesian total stress σ'yy – cross section @y=0,41m - CA-01-C1-T (embankment: crushed rock; subsoil: clay; pile head: fixed)

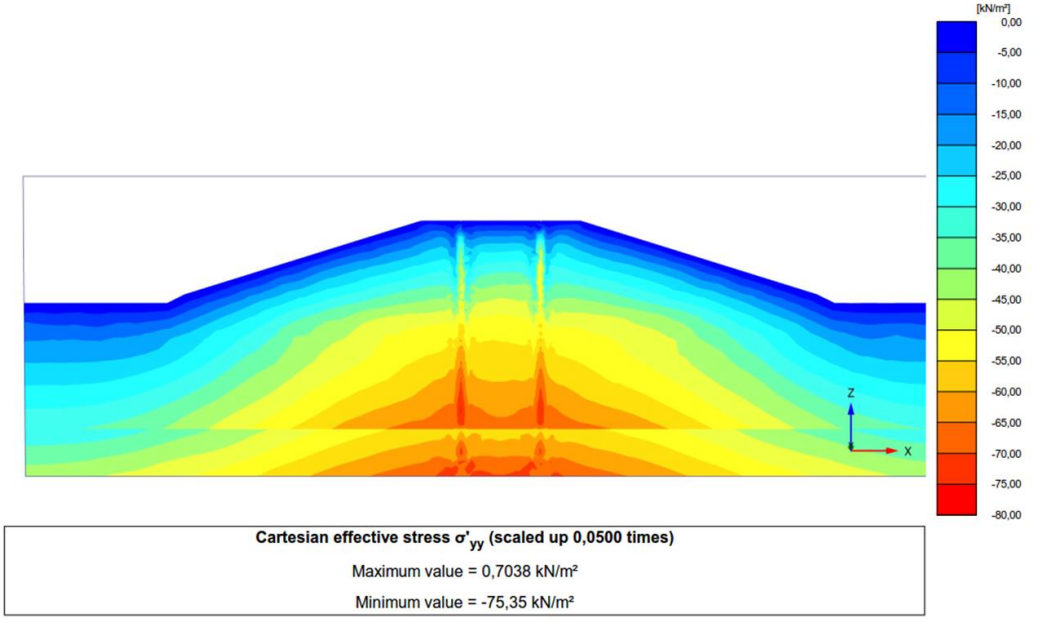

Figure 6-33 Cartesian effective stress σ'yy – cross section @y=0,41m - CA-02-S1-T (embankment: sand; subsoil: sand; pile head: fixed)

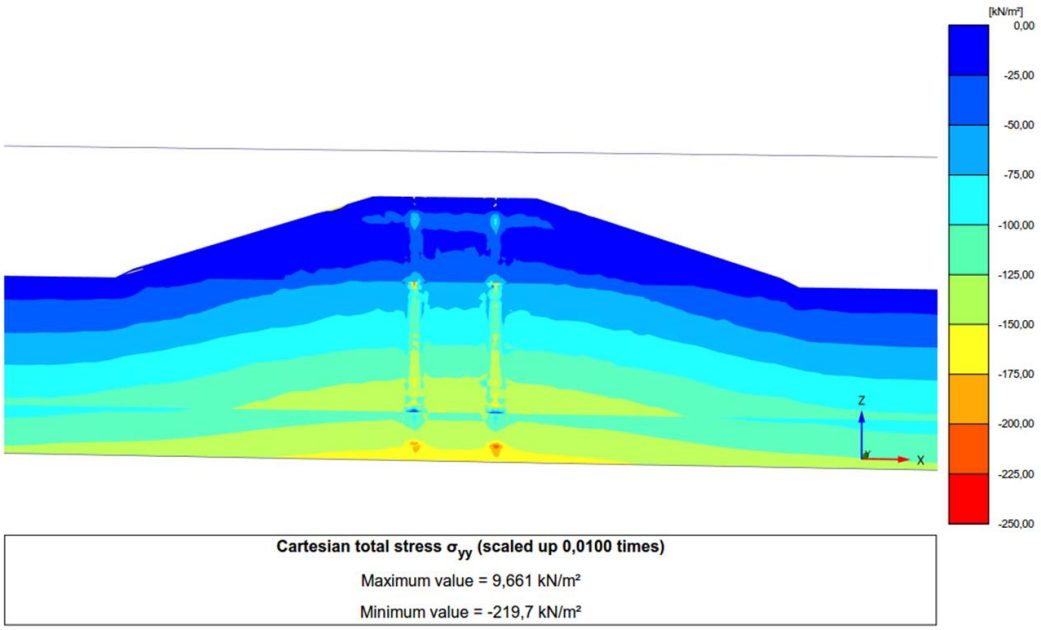

Figure 6-34 Cartesian total stress σ'yy – cross section @y=0,41m - CA-02-C1-T (embankment: sand; subsoil: clay; pile head: fixed)

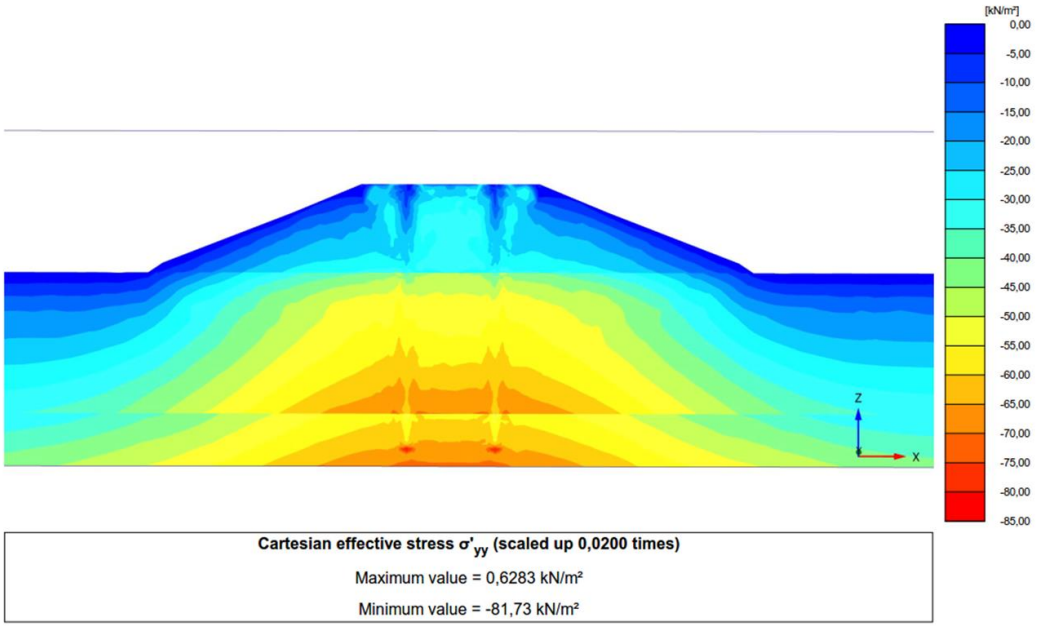

Figure 6-35 Cartesian effective stress σ'yy – cross section @y=0,41m - NCA-01-S1-T (embankment: crushed rock; subsoil: sand; pile head: fixed)

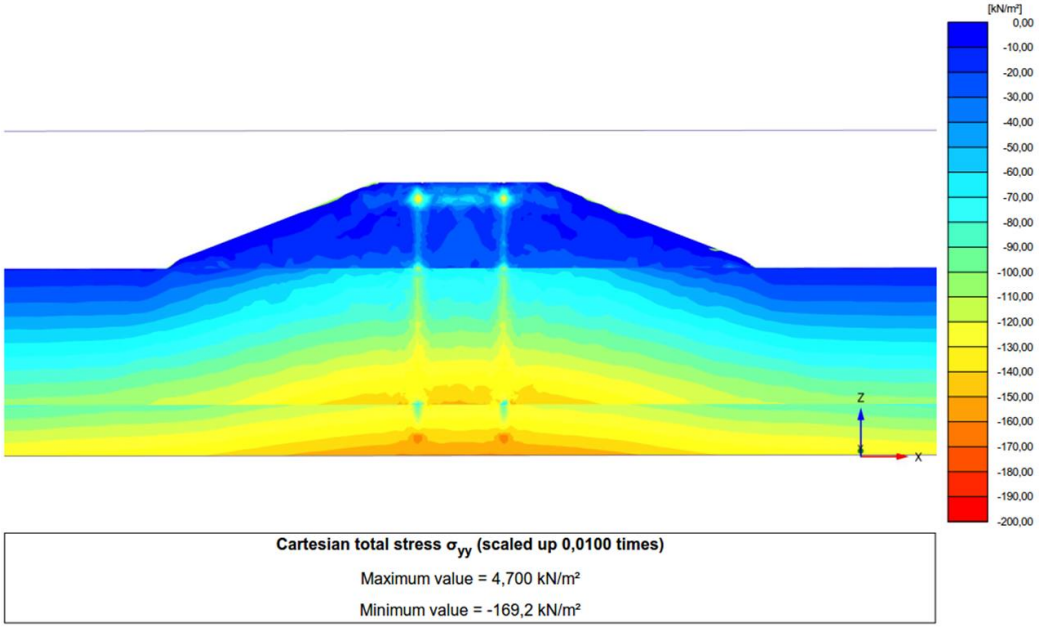

Figure 6-36 Cartesian total stress σ'yy – cross section @y=0,41m - NCA-01-C1-T (embankment: crushed rock; subsoil: clay; pile head: fixed)

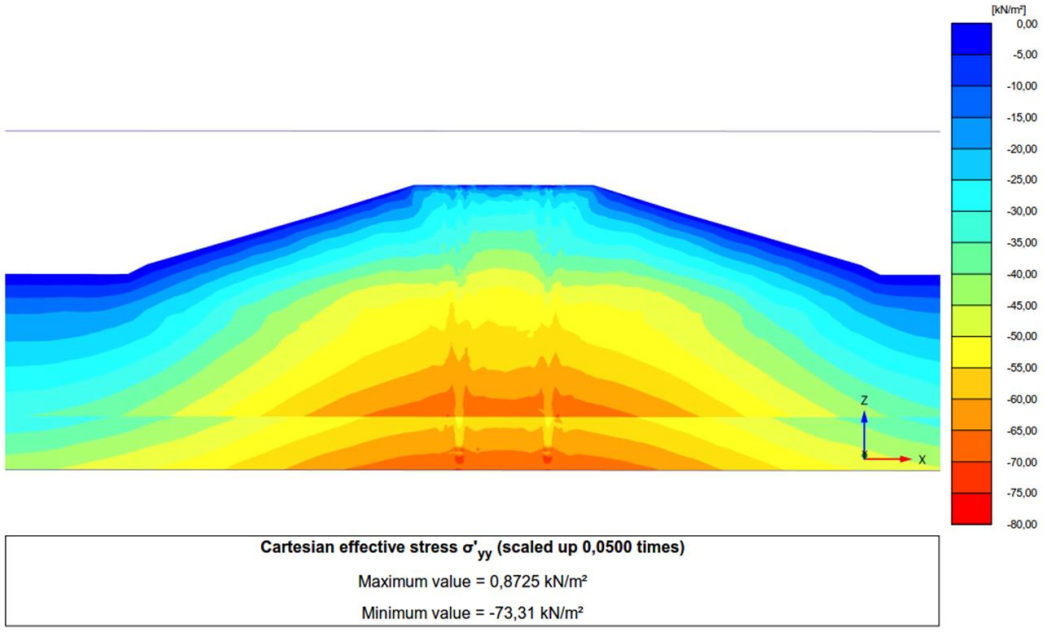

Figure 6-37 Cartesian effective stress σ'yy – cross section @y=0,41m - NCA-02-S1-T (embankment: sand; subsoil: sand; pile head: fixed)

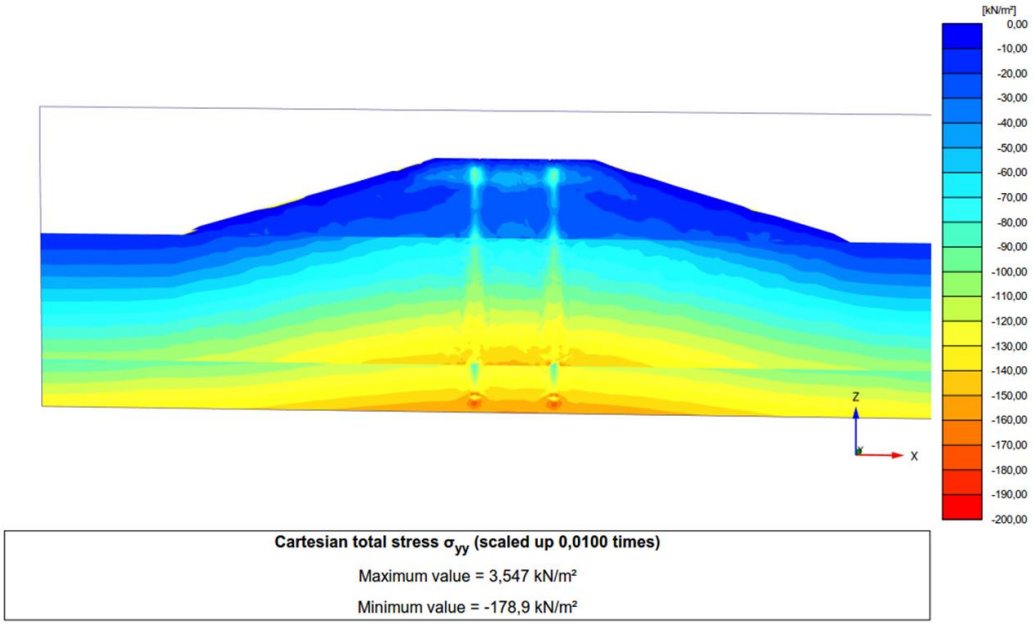

Figure 6-38 Cartesian total stress σ'yy – cross section @y=0,41m - NCA-02-C1-T (embankment: sand; subsoil: clay; pile head: fixed)

Figure 6-39 shows a comparison between the computed FE earth pressure and the analytical solution for a CA case with crushed rock embankment, fixed pile head and sand vs clay subsoil. Figure 6-39 further includes the earth pressure between the piles, extracted from a line section taken at equal distance from the piles centrelines @[x=0, y=0, z=0/-18] and the earth pressure for the case where piles are not modelled.

As anticipated, the earth pressure between the piles is lower than the average earth pressure acting along the piles. Further, it is consistent with the earth pressure computed for the case where piles are not present. For the CA-01-S1-T case (sand subsoil), the earth pressures are in line with the analytical solution below z=-6m. At the same depths, the analytical solution seems to under-estimate the earth pressure in the clay subsoil (CA-01-C1-T).

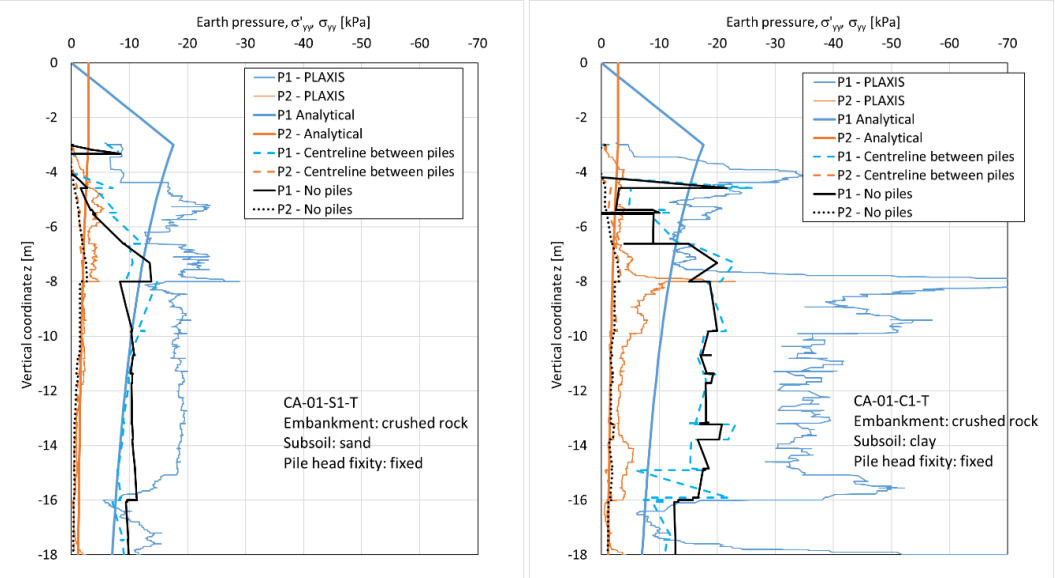

Figure 6-39 FE vs analytical earth pressure solution for CA-01-S1-T and CA-01-C1-T – comparison with earth pressure between piles and earth pressure without piles (embankment: crushed rock; subsoil: sand/clay; pile head: fixed)

7 Improvement of analytical solutions for earth pressure

The FE results seems to suggest that the current analytical approach does not provide with a realistic estimate of earth pressure increments, especially in undrained conditions. An attempt to improve the current analytical solution is presented here.

A new set of equations for earth pressure increments P1 and P2 is proposed as follows (equations (12)-(15) and Figure 7-1):

$$P1\,(kPa) = \gamma \cdot H \cdot K_o \quad (12)$$

$$P1'\,(kPa) = \gamma \cdot H \cdot [B/(B+z)] \cdot K_o^i \cdot f \quad (13)$$

$$P2\,(kPa) = q \cdot K_o \quad (14)$$

$$P2'\,(kPa) = q \cdot [B/(B+z)] \cdot K_o^i \cdot f \quad (15)$$

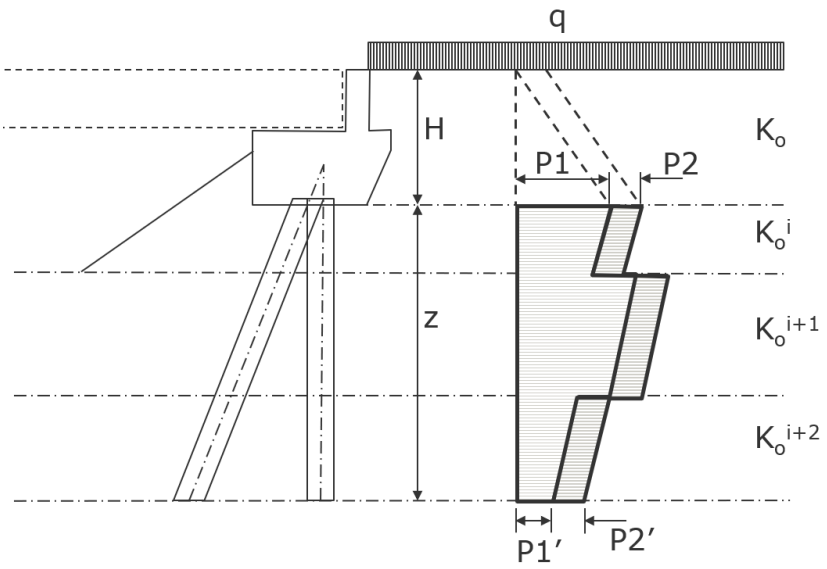

Figure 7-1 Illustration of improved analytical solution accounting for the variation of K_o in each layer or with depth.

P1 and P2 represent the earth pressure increment values at pile head level (z=H) induced by the superstructure and traffic load, respectively. The notation for P1, P1', P2 and P2' is retained from the 2007 solution, but the traffic load symbol is changed to "q" for clarity. B is the width of the top of the embankment. The symbol *f* is a model factor (see below).

The logic behind these equations considers the specific K_o to each soil layer (K_o^i), or a K_o that varies with depth. So, for each layer *i*, the vertical stress increment is multiplied by the layer-specific or depth dependent K_o^i value. Under drained conditions, normally $K_o \approx 1 - \sin\varphi'$; while for undrained conditions, $K_o = 1$, which reflects the condition $\varphi = 0$.

Figure 7-2 and Figure 7-3 illustrate a comparison between the calculation results for CA-01-S1-T, CA-01-C1-T, NCA-01-S1-T and NCA-01-C1-T and the original and suggested improved solution for earth pressure. The curves representing the original solution from 2007 account for the gathering effect of earth pressure over an area equal to 3 times the pile diameter (section 0). Therefore, a factor of 3 is applied to the basic curves, unlike in the previous sections. The 2007 solution curves are cut here at 1,2h (embankment height including the superstructure h=8m) from the top of the superstructure at -9,6m, as suggested in the 2007 guide.

For the calculation of P2, a uniformly distributed road traffic load of q = 10 kPa was used. This is an averaged value that corresponds to the NCCI7 road traffic load. It has been established that the basic behaviour of the FE model is similar with both road traffic and train loads, so only road traffic loads were used in this verification.

Unlike the original solution, the improved solution appears to be able to capture the earth pressure, especially in the undrained clay subsoil. In particular, the original solution overestimates the earth pressure in the drained layer above z=-9,6m. In presence of undrained layers, the 2007 solution may underestimate earth pressure. Further, the FE results suggest that earth pressure develops below a depth of 1,2h. Therefore, it is not negligible as suggested by the current approach.

For the CA cases, a model factor f=1,3 appears to provide a reasonable fit to the computed earth pressure. For NCA, f=1 can be assumed. These model factors may change if pile spacing and geometry deviate from those considered in this study.

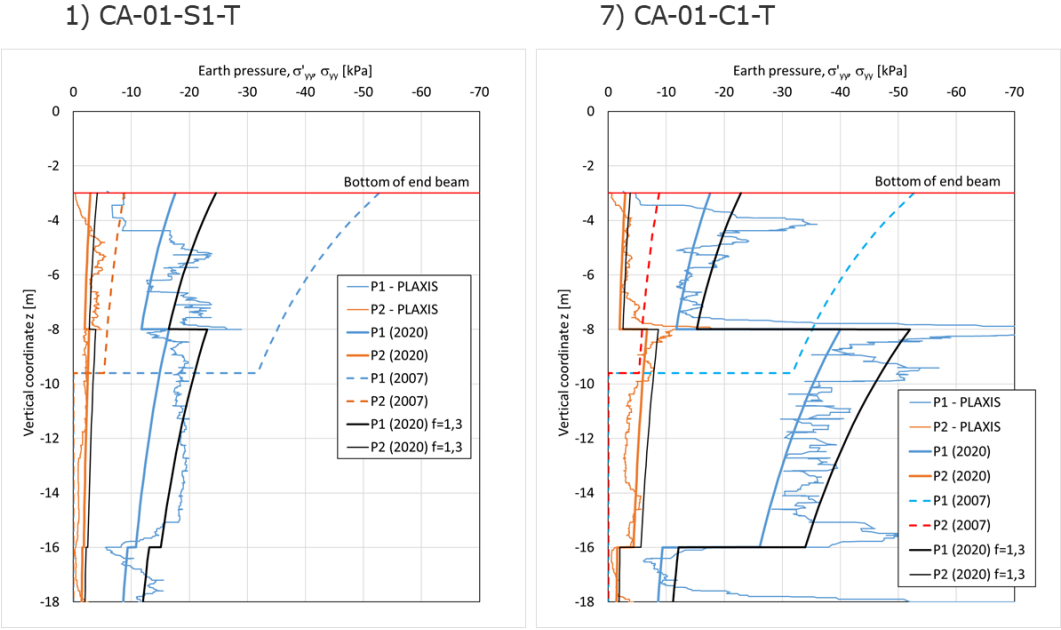

Figure 7-2 Comparison of calculation results and original (2007) and improved analytical solution for CA-01-S1-T and CA-01-C1-T (embankment: crushed rock; subsoil: sand/clay; pile head: fixed; road traffic load)

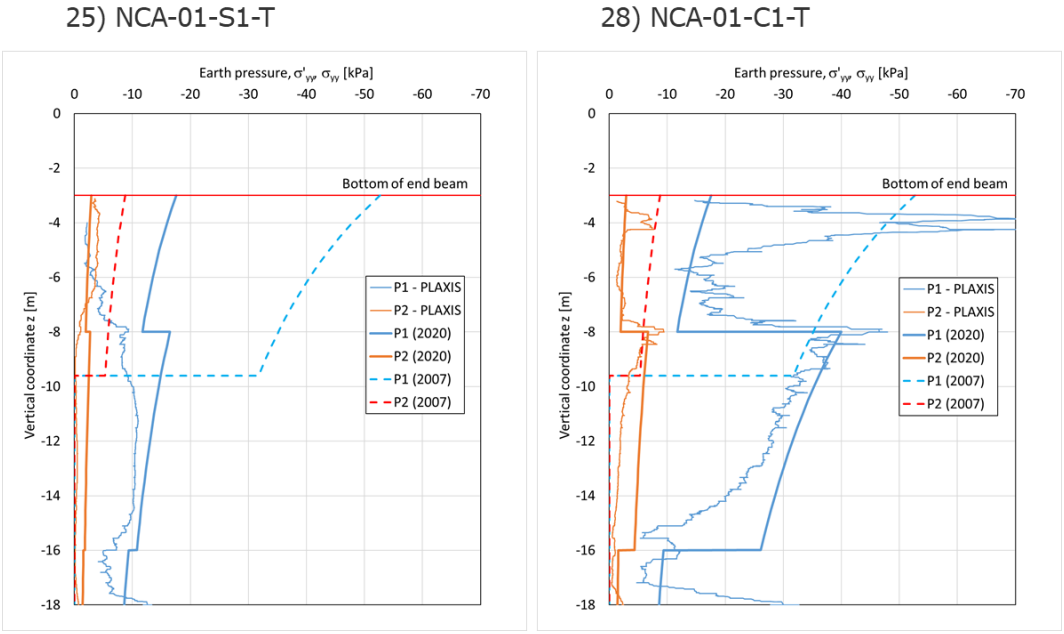

Figure 7-3 Comparison of calculation results and original (2007) and improved analytical solution for NCA-01-S1-T and NCA-01-C1-T (embankment: crushed rock; subsoil: sand/clay; pile head: fixed; road traffic load)

8 Discussion

8.1 Using the results of this study when modelling a pile slab

In presence of a pile slab, the embankment and superstructure are expected to develop smaller deformations than those observed in this study. Under these conditions, the mobilized earth pressure may be close to a K_o condition. As the pile slab supports the superstructure and traffic load, only little earth pressure loading is expected to act on the bridge piles below the slab. No attempt to estimate such earth pressure values can be made here.

8.2 Limitations of this study

This study provided insights into the modelling of earth pressure on bridge abutment piles and compared a 3D numerical to a simple analytical solution. Nevertheless, the use of FE results needs thoughtful judgment, given the following limitations:

- The results are valid for the geometries and conditions analysed. Results may differ when pile spacing, pile diameter, abutment geometry, thickness of the different layers, position of ground water table and construction phases deviate from the assumptions made in this study.

- The earth pressure on piles is modelled from the normal stress acting on a surface normal to the principal deformation direction of the pile. A full integration of the stresses acting on the soil-pile interface may provide with more accurate results. Nevertheless, Ramboll's experience suggests that the computed average earth pressures should not deviate significantly from those obtainable from more advanced integration methods.

- Piles are modelled as linear elastic and, therefore, possible yielding cannot be captured by the model. However, correctly designed piled foundations are not loaded close to yielding in any case.

- Input parameters were determined as "best estimate" parameters based on literature and experience. No sensitivity study was performed to evaluate the effect of the single parameters on the numerical results. In general, a proper parameter assessment would require a comprehensive testing (laboratory/ in-situ) campaign to characterize the different soil units involved in the soil-structure interaction problem. Further, low and high boundaries of soil properties should be selected accordingly with the design requirements and codes.

- The clay subsoil is modelled assuming an isotropic undrained shear strength (s_u) and a constant shear modulus that is independent of the shear mobilization in the soil. These assumptions are not realistic (they may be under specific circumstances), as both s_u and stiffness of Finnish clays are known to be stress-path dependent (or anisotropic) (e.g. Lehtonen 2015;

Mansikkamäki 2015; D'Ignazio 2016). Further, assuming a constant s_u may not reflect the stress state and over-consolidation throughout the model domain.

- In presence of clay subsoil, it is crucial to model the correct construction stages of the embankment and superstructure, including possible preloading phases. This will provide accurate modelling of shear mobilization in both coarse and clay layers. In this study, it is assumed that the embankment is built on the virgin soil prior to the application of the superstructure and the loads, simulating a long-term condition. While the response under the external traffic/train loads is substantially undrained, drainage and consolidation are expected to occur during the construction phases of the superstructure. Therefore, the computed earth pressure resulting from the superstructure load (P1) should be intended as the upper boundary associated with the given set of parameters.

9 Summary, conclusions and recommendations for future research work

9.1 Summary and conclusions

This study focused on modelling earth pressure from traffic and train loads on abutment piles of integral bridges. Two different bridge abutment configurations have been analysed: bridge with cantilever span (CA) and bridge without cantilever span (NCA). The main scope of the study was to compare the analytical solution from Tiehallinto (2007), which is used in bridge geotechnics in Finland, with the earth pressure computed from 3D Finite Element analyses using the Bentley Plaxis 3D program.

The 2007 analytical solution gives the earth pressure based on the earth pressure coefficient at rest (K_o) and the weight of the embankment/super-structure material located above the pile heads, assuming a 2:1 stress distribution with depth. Further, the solution assumes that the earth pressure is gathered from a 3-pile-diameter width, meaning that the analytical curves should be multiplied by a factor of three, and that the earth pressure is negligible below a certain depth according to the thickness of the embankment and superstructure.

The scope of the FE analyses was to study the effect of using different bridge configurations, different embankment materials and slope geometries, subsoils (clay, soft vs sand, stiff) and pile bearings (fully fixed vs free pile head) on the earth pressure under traffic and train loads.

Coarse (drained) layers were modelled with the Hardening Soil model, which uses a stress-dependent stiffness and can model hardening along with plastic straining. The Mohr-Coulomb model with a given undrained shear strength and a constant shear stiffness was used for the undrained clay subsoil. Piles were modelled as volume elements with linear elastic behaviour, with interface elements that ensure strength reduction at the soil-pile interface compared to the surrounding soil.

Ramboll selected appropriate models and input parameters based on recommendations from Väylä, available literature and in-house experience. The parameters are meant to represent a best estimate of the soil properties. Therefore, the modelled earth pressures are also intended to represent best estimates.

Results show that in most cases the 2007 analytical solution appears to deviate from the FE results. The discrepancies are mainly evident in undrained conditions, where the analytical solution notably underestimates the earth pressure. The analytical solution seems to agree with the numerical results when the model behaviour is governed by drained conditions (i.e. with stiff sand subsoil). Nevertheless, this could be anticipated given its formulation. It must be pointed out that the analytical curves were not multiplied by a factor of 3 to account for the stress gathering effect behind the piles. This would have led to a severe overestimation of earth pressure, especially in the coarse layers. In the

FE results, such a "gathering effect" for earth pressure was not visible. Moreover, earth pressure appears to develop over the entire pile length, in contrast with the recommendations given in previous guidelines.

In general, the Tiehallinto (2007) analytical solution (when including the factor of 3 and the depth cut-off) seems to:

- overestimate the earth pressure increment in drained conditions,
- underestimate the earth pressure increment in undrained conditions, and
- fully underestimate the earth pressure below a depth of 1,2 times embankment height

In undrained conditions, the two solutions diverge even in the drained layers, especially for the NCA cases with clay subsoil. This may be explained by the high shear mobilization in the embankment that results from the simulation of long-term conditions (large settlement after construction). The embankment and superstructure show a softer behaviour compared to the case with stiff (sand) subsoil, with consequent stress concentration behind the rigid piles. This behaviour seems to be less pronounced in the CA model with fixed pile-head, while it tends to disappear when the pile head is free to move (no bearing). However, the comparison between CA and NCA is not straightforward, given the differences in the geometry, especially in terms of distance between the piles and the abutment rigid wall and location of the pile head fixity.

Finally, a way to improve the current analytical solution was proposed based on the FE results. The improved solution accounts for the K_o of the different soil layers and it assumes $K_o = 1$ in undrained conditions. The latter is in line with basic earth pressure theory. Compared to the standard solution, the improved solution appears to be able to capture the earth pressure in the undrained layers. For the drained layers, the benefit is less evident, as some discrepancy remains between the analytical and the numerical results. In order to obtain a better fit to the computed earth pressure, model factors are proposed for CA and NCA to. For CA, the calculated earth pressure needed to be multiplied by a factor of 1,3; while for NCA this factor could be taken equal to 1. Therefore, the multiplying factor of 3 recommended in Tiehallinto (2007) appears to be conservative when applied along with the improved solution. Further, the earth pressure seems to develop over the entire pile length. Note that these conclusions and proposed model factors are only valid for the pile spacing, geometry and construction phases adopted in this study.

9.2 Recommendations for future research work

It would be of valuable importance in future research to:

- Evaluate the effects of geometry, including pile spacing, pile diameter and thickness of the soil units on the calculated earth pressure.

- Evaluate the effect of different construction phases; i.e. evaluating the effect of constructing the embankment and superstructure before or after pile installation; evaluating the effect of preload and consolidation in presence of clay subsoil.

- Evaluate the effect of forces acting on piles (axial, horizontal and bending) caused by bridge superstructure and loading.

- Evaluate the effect of soil parameters on the model behaviour and perform a parametric study to evaluate the impact of each model parameter on the earth pressure. Possibly, include small strain behaviour for both coarse and fine-grained layers.

- Use advanced soil models for clay to model strength and stiffness anisotropy, shear mobilization and change of anisotropy in the soil. For instance, the SHANSEP-NGI-ADP model (Panagoulias et al. 2018) or the effective stress based SCLAY1 or SCLAY-1S model (Karstunen et al. 2005). These models would require a proper laboratory calibration, even though literature exists on their use in Finnish soil conditions (e.g. Mansikkamäki 2015; D'Ignazio 2016). When using advanced models, it is crucial to associate a detailed modelling of all the construction phases of the embankment and superstructure over the clay layer(s) (i.e. preloading and consolidation). The models will then predict undrained behaviour based on the current stress state and shear mobilization in the soil.

- Study the effect of using different FE models on earth pressure. For instance, compare the Hardening Soil (HS) with Hardening Soil with small strain (HSsmall) and Mohr-Coulomb with the clay models mentioned above.

- If available, back-calculate monitoring data from existing structures to validate the model's performance.

References

D'Ignazio, M. (2016). Undrained shear strength of Finnish clays for stability analyses of embankments. PhD thesis, Tampere University of Technology, Tampere. Publication 1412

Janbu, N. (1998). Sediment deformations. University of Trondheim, Norwegian University of Science and Technology, Geotechnical Institution. Bulletin, 35, 86.

Karstunen, M., Krenn, H., Wheeler, S. J., Koskinen, M., & Zentar, R. (2005). Effect of anisotropy and destructuration on the behavior of Murro test embankment. International Journal of Geomechanics, 5(2), 87-97.

Lehtonen, V. (2015). Modelling undrained shear strength and pore pressure based on an effective stress soil model in limit equilibrium method. PhD thesis, Tampere University of Technology, Tampere. Publication 1337.

Liikennevirasto (2017). Eurokoodin soveltamisohje – Geotekninen suunnittelu – NCCI 7. Siltojen ja pohjarakenteiden suunnitteluohjeet 21.4.2017. Liikennevirasto ohjeita 13/2017.

Liikennevirasto (2018). RATO 3. Ratatekniset ohjeet (RATO) osa 3, radan rakenne. Liikennevirasto ohjeita 13/2018.

Mansikkamäki, J. (2015). Effective stress finite element stability analysis of an old railway embankment on soft clay. PhD thesis, Tampere University of Technology, Tampere. Publication 1287.

Panagoulias, S., Vilhar, G., Brinkgreve, R. B. J. (2018) The SHANSEP NGI-ADP model 2018. Plaxis B.V., The Netherlands.

PLAXIS (2020). Bentley Plaxis user's manual (www.plaxis.nl)

Termaat, R.J., Vermeer, P.A., Vergeer, C.J.H. (1985). Failure by large plastic deformations. In Proceedings of the 11th International Conference on Soil Mechanics and Foundation Engineering, San Francisco, 12-16 Aug

Tiehallinto (2007). Sillan geotekniset suunnitteluperusteet. Suunnitteluvaiheen ohjaus. Tiehallinto, Helsinki.

Väylä (2020). Liikuntasaumattoman sillan suunnittelu, Väyläviraston ohjeita X/2020 (Draft version/early 2020)

Finnish Transport
Infrastructure Agency

ISSN 2490-0745
ISBN 978-952-317-785-7
www.vayla.fi